Mitogen-activated protein kinase phosphatase-2 deletion modifies ventral tegmental area function and connectivity and alters reward processing.

Karolina Pytka[1,2], Neil Dawson[1,3], Kyoko Tossell[4,5], Mark A. Ungless[4,5], Robin Plevin[1], Ros R. Brett[1] and Trevor J. Bushell[1*]

[1] Strathclyde Institute of Pharmacy & Biomedical Sciences, University of Strathclyde, 161 Cathedral Street, Glasgow, G4 0RE, UK,

[2] Department of Pharmacodynamics, Faculty of Pharmacy, Jagiellonian University Medical College, Medyczna 9, 30-688 Krakow, Poland,

[3] Division of Biomedical and Life Sciences, Lancaster University, Lancaster, LA1 4YQ, UK,

[4] MRC London Institute of Medical Sciences (LMS), Du Cane Road, London W12 0NN, UK

[5] Institute of Clinical Sciences (ICS), Faculty of Medicine, Imperial College London, Du Cane Road, London W12 0NN, UK

*Corresponding author:

T.J. Bushell, Strathclyde Institute of Pharmacy & Biomedical Sciences, University of Strathclyde, 161 Cathedral Street, Glasgow G4 0RE, UK. Tel: 0141 548 2856, Fax: 0141 552 2562, Email: trevor.bushell@strath.ac.uk

Running title: MKP-2 deletion alters VTA function and connectivity.

Number of pages: 31 Number of figures: 4 Number of tables: 2 Supplementary table: 1

Number of words: i) whole manuscript 7577 ii) Abstract: 219.

Keywords: mitogen-activated protein kinase phosphatase-2, local cerebral glucose utilization, spontaneous excitatory postsynaptic current, sucrose preference, amphetamine-induced hyperlocomotion.

K.P. and N.D. contributed equally to this work.

ABSTRACT

Mitogen-activated protein kinases (MAPKs) regulate normal brain functioning and their dysfunction is implicated in a number of brain disorders. Thus, there is great interest in understanding the signalling systems that control MAPK functioning. One family of proteins that contribute to this process, the mitogen-activated protein kinase phosphatases (MKPs), directly inactivate MAPKs through dephosphorylation. Recent studies have identified novel functions of MKPs in foetal development, the immune system, cancer and synaptic plasticity and memory. In the present study, we performed an unbiased investigation using MKP-2$^{-/-}$ mice to assess whether MKP-2 plays a global role in modulating brain function. Local cerebral glucose utilization is significantly increased in the ventral tegmental area (VTA) of MKP-2$^{-/-}$ mice, with connectivity analysis revealing alterations in VTA functional connectivity, including a significant reduction in connectivity to the nucleus accumbens and hippocampus. In addition, spontaneous excitatory postsynaptic current frequency, but not amplitude, onto putative dopamine neurons in the VTA is increased in MKP-2$^{-/-}$ mice, which indicates that increased excitatory drive may account for the increased VTA glucose utilization. Consistent with modified VTA function and connectivity, in behavioural tests MKP-2$^{-/-}$ mice exhibited increased sucrose preference and impaired amphetamine-induced hyperlocomotion. Overall, these data reveal that MKP-2 plays a role in modulating VTA function and that its dysfunction may contribute to brain disorders in which altered reward processing is present.

ABBREVIATIONS

^{14}C-2-DG - ^{14}C-2-deoxyglucose

ACSF - artificial cerebrospinal fluid

BDNF - brain-derived neurotrophic factor

BSA - bovine serum albumin

CNS - central nervous system

DA - dopamine

DUSP - dual-specificity phosphatases

ERK - extracellular signal related kinase

FBS - fetal bovine serum

JNK - c-jun N-terminal kinase

LCGU - local cerebral glucose utilization

MAPK - mitogen-activated protein kinase

MKP - mitogen-activated protein kinase phosphatase

NDS – normal donkey serum

PLSR - partial least squares regression algorithm

PBS - phosphate-buffered saline

PFA - paraformaldehyde

RoI - region of interest

sEPSC - spontaneous excitatory postsynaptic current

SPT - sucrose preference test

TH - tyrosine hydroxylase

VIP - variable importance to the projection

VTA - ventral tegmental area

1 | INTRODUCTION

The mitogen-activated protein kinases (MAPK) form a family of evolutionally conserved proteins, which play a critical role in various cellular processes including cellular proliferation, differentiation, development, transformation and apoptosis (Keshet and Seger, 2010). The mammalian MAPK family consists of the extracellular signal related kinase (ERK), the c-jun N-terminal kinase (JNK) and p38 MAPK. MAPK signalling shares a common three-tiered core structure, where the activation of MAPK requires sequential phosphorylation and activation of each component kinase. The activated MAPKs then convert the extracellular stimuli into a broad range of cellular responses. In the central nervous system (CNS), MAPKs are expressed in numerous cell types, where they play a role in the regulation of synaptic transmission and plasticity (Thomas and Huganir, 2004; Samuels *et al.,* 2009). In addition, their dysfunction has been implicated in CNS disorders including Alzheimer's disease, autism, Parkinson's disease, anxiety and addiction (Yasuda et al., 2011; Lee & Kim, 2017; Vithayathil et al., 2018).

The duration and magnitude of MAPK activation are crucial in determining the physiological outcome of this signalling pathway (Marshall, 1995; Caunt & Keyse, 2013). Thus, the negative regulation of phosphorylation process is vital for controlling MAPK signalling. The process of MAPK inactivation is mediated by the family of dual-specificity phosphatases (DUSPs), the mitogen-activated protein kinase phosphatases (MKPs), which catalyse the dephosphorylation of MAPK that consequently leads to inhibiting their activity. However, our knowledge of MKP function in the CNS is limited but studies suggest a role for the prototypic *Dusp1* (MKP-1) in brain-derived neurotrophic factor (BDNF)-induced axonal branching (Jeanneteau *et al*., 2010) and depression (Duric et al., 2010; Chen et al., 2012; Jia et al., 2013; Hui et al., 2016; Barthas et al., 2017). In contrast, the role of *Dusp4* (MKP-2) in the CNS has not been studied extensively. However, we have recently shown that *Dusp4* deletion increases hippocampal

spontaneous excitatory postsynaptic potential (sEPSC) frequency as well as impairing spatial reference and working memory (Abdul Rahman et al., 2016).

Building on our previous findings and given our limited knowledge of MKP-2 function in the CNS, we performed an unbiased investigation using MKP-2$^{-/-}$ mice to examine the consequence of *Dusp4* gene deletion on brain function and behaviour.

2 | MATERIALS AND METHODS

2.1 | Animals

All *in vivo* experimental procedures were in accordance with UK legislation (Animals (Scientific Procedures) Act 1986) and with approval by the University of Strathclyde Ethics Committee. All experiments were completed using male MKP-$2^{+/+}$ and MKP-$2^{-/-}$ mice generated as previously described (Al-Mutairi et al., 2010), normally group-housed (5–6 per cage) under standard conditions (21°C, 45%–65% humidity, 12h dark/light cycle [lights on 06:00]) in cages provided with environmental enrichment in the form of a plastic refuge and nesting material. Animals had free access to food and water with all behavioural procedures carried out between 09.00 and 17.00. Mice were randomly assigned to the treatment groups with the experimenter blinded to each group.

2.2 | ^{14}C-2-Deoxyglucose (^{14}C-2-DG) functional brain imaging

Local cerebral glucose utilization (LCGU) was determined in MKP-$2^{-/-}$ (n = 11) and MKP- $2^{+/+}$ (n = 10) mice (10-12 weeks old) in accordance with previously published protocols , using an approach adapted from the original protocol developed in rats (Sokoloff et al., 1977) for application in conscious freely-moving mice (Dawson et al., 2011, 2013). In brief, LCGU measurement was initiated by injection of ^{14}C-2-DG (*intraperitoneally* (*i.p.*), 4.625 MBq/kg in physiological saline at 2.5ml/kg (Perkin-Elmer, UK) and animals were returned to their home cage. Forty five minutes after ^{14}C-2-DG injection animals were decapitated and a terminal blood sample collected, by torso inversion, into heparinized weigh boats. Plasma glucose concentrations (mmol/L) were detected from whole blood using a blood glucose monitor (Accu-Chek Aviva). The brain was then rapidly dissected out intact, frozen in isopentane (-40°C) and stored at (-80°C) until sectioning. Blood samples were centrifuged to isolate plasma, and plasma ^{14}C concentrations (20µl) were determine by liquid scintillation analysis (Packard).

Frozen brains were sectioned (20µm) in the coronal plane in a cryostat (-20°C). A series of three consecutive sections were retained from every 60µm, thaw mounted onto slide covers and rapidly dried on a hotplate (70°C). Autoradiograms were generated by apposing these sections, together with precalibrated ^{14}C standards (39-1098 nCi/g tissue equivalents, Amersham International, UK) to x-ray film (Carestream BioMax MR film, Sigma-Aldrich, UK) for 7 days. Autoradiographic images were analysed by a computer based image analysis system (MCID/M5+, Interfocus, UK). The local isotope concentration for each brain region of interest (RoI) was derived from the optical density of the autoradiographic images relative to that of the coexposed ^{14}C standards, with 8-12 replicate measurements taken per RoI in each animal. LCGU was determined in 53 anatomically distinct brain RoI as the ratio of ^{14}C present in that region relative to the average ^{14}C-2-DG concentration in the whole brain of the same animal, referred to as the ^{14}C-2-DG uptake ratio. There was no significant difference between the whole brain average ^{14}C-2-DG concentration in MKP-2$^{-/-}$ mice relative to wild-type controls (MKP-2$^{+/+}$ 142.05 ± 7.74 nCi/g; MKP-2$^{-/-}$ 164.80 ± 8.27 nCi/g, p=0.103 Student's t-test), suggesting that MKP-2 deletion did not significantly impact global cerebral metabolism. In addition, there was no significant difference in plasma ^{14}C-2-DG levels (MKP-2$^{+/+}$ 22.9 ± 1.58 nCi/ml, MKP-2$^{-/-}$ 29.21 ± 3.33 nCi/ml, p=0.115 Student's t-test) or glucose levels (MKP-2$^{+/+}$ 9.00 ± 0.35 mmol/L, MKP-2$^{-/-}$ 8.28 ± 0.46 mmol/L, p=0.224 Student's t-test) between the two experimental groups, suggesting that there were no systematic difference in plasma glucose or ^{14}C-2-DG concentrations between the two experimental groups that might impact on LCGU measurement.

2.3 | Functional brain connectivity analysis using PLSR

The partial least squares regression algorithm (PLSR) was employed to define significant differences in the functional connectivity of selected "seed" RoI to all other RoI analysed from the functional ^{14}C-2-DG brain imaging data, as previously outlined (Dawson et al., 2012, 2013;

Hughes et al., 2019), and was undertaken using the PLS package (Mevik and Wehrens, 2007) in R (R Core Team, 2018). The analysed "seed" brain RoI were those regions in which a significant alteration in overt LCGU was observed, namely the ventral tegmental area (VTA, Figure 1). In brief, functional connectivity between the "seed" RoI and all other RoI analysed was defined by the variable importance to the projection (VIP) statistic gained from the PLSR models. A region was considered to be functionally connected to the "seed" region if the 95% confidence interval (95% CI) of the VIP statistic exceeded 0.8. This denotes a considerable contribution of the explanatory variable (RoI metabolism) to the dependent variable ("seed" RoI metabolism) in PLSR models. The standard deviation (SD) and 95% CI of the VIP statistic were estimated by jack-knifing. Significant differences in the VIP statistic between groups were analysed using t-test with Bonferroni *post-hoc* correction for multiple comparisons on the basis of the number of potentially connected RoI (52). Thus genotype-induced alterations in regional functional connectivity to the VTA were defined in terms of lost (VIP 95% CI >0.8 in MKP-$2^{+/+}$ mice, VIP 95% CI <0.8 in MKP-$2^{+/-}$ mice and $p<0.05$ significant difference between genotypes) and abnormally gained (VIP 95% CI <0.8 in MKP-$2^{+/+}$ mice, VIP 95% CI >0.8 in MKP-$2^{+/-}$ mice and $p<0.05$ significant difference between genotypes) connectivity in MKP-$2^{-/-}$ mice.

2.4 | Electrophysiology

Mice (19–25 days old) were killed by cervical dislocation and decapitated. The brains were rapidly removed and placed immediately in an ice-cold (0–3°C), oxygenated (95% O_2/5% CO_2) artificial cerebrospinal fluid (ACSF) containing (in mM): 124 NaCl, 3 KCl, 26 $NaHCO_3$, 2.5 NaH_2PO_4, 2 $MgSO_4$, 2 $CaCl_2$, 10 glucose. Horizontal slices (230 μm) were cut using a vibratome and transferred to a holding chamber containing oxygenated ACSF, equilibrated at 37°C for 30 min followed for 30 min at the room temperature prior to recording. Slices were

then transferred into a submerged recording chamber continuously perfused with ACSF at a flow rate at 2-3 mL min^{-1} at room temperature. Electrodes (4-7 MΩ) were filled with an internal solution containing (in mM): 130 $KMeSO_4$, 20 KCl, 4 Mg-ATP, 0.4 Na-GTP, 0.5 EGTA, 10 HEPES, 0.5% (w/v) biocytin, pH 7.2, 290 mOsm. Visually-guided whole-cell patch-clamp recordings were made from neurons in the VTA using an Axopatch 200B amplifier (Molecular Devices, USA), connected to a personal computer interfaced with Digidata 1322A interface (Molecular Devices, USA) and captured using pClamp9.0 software (Molecular Devices, USA). Spontaneous EPSCs were recorded at -70mV for 5 min periods, digitized at 5kHz. For I_H recordings, cells were held at -70mV in voltage clamp mode with -10mV increments at 10s intervals. Data were analysed offline using pClamp9.2 software (Molecular Devices, USA) or MiniAnalysis software (Synaptosoft, USA). For all slice experiments, n is equal to one neuron per slice per animal with all I_H positive neurons confirmed to be dopaminergic (DAergic) neurons post experiment using immunohistochemistry (see below).

2.5 | Immunohistochemistry

2.5.1 | Confirmation of VTA dopamine (DA) neuron identity

Immediately following electrophysiological experiments, each slice was fixed in 4% paraformaldehyde (PFA) for 1 h, then washed with phosphate-buffered saline (PBS). Slices were then agitated in PBS with 1% Triton X-100 for 1 h. Free-floating slices were then pre-blocked for 1 h at room temperature in PBS with 0.5% Triton X-100, 1% (w/v) bovine serum albumin (BSA) and 5% (v/v) fetal bovine serum (FBS) and incubated overnight at 4°C with chicken polyclonal anti-tyrosine hydroxylase (TH) antibody (1:500, Abcam, ab76442) with 0.5% Triton X-100, 1% (w/v) BSA and 5% (v/v) FBS. Slices were rinsed in PBS and incubated for 3 h with goat anti-chicken Alexa Fluor™ 555 (1:200, Life Technologies, A21437) and streptavidin-Alexa Fluor™ 488 (1: 500, Life Technologies, S11223) with 0.5% Triton X-100,

1% (w/v) BSA and 5% (v/v) FBS. After subsequent PBS rinses, slices were mounted on slides using Vectashield anti-fade mounting medium with DAPI (Vector Laboratories) and visualized using a Leica SP5 confocal laser-scanning microscope.

2.5.2 | VTA structure

Male MKP-2$^{-/-}$ and MKP-2$^{+/+}$ mice (10-12 weeks old, n=6 for both genotypes) were perfused transcardially with 4% PFA. Brains were removed and post-fixed for 1 hour in 4% PFA, washed with PBS, followed by cryoprotection in 30% sucrose. Coronal brain sections (70µm) were prepared using a cryostat (Leica). Slices were rinsed with PBS and agitated in PBS with 0.5% Triton X-100 for 15 min. Free-floating sections were then pre-blocked for 1 hour at room temperature in PBS with 0.2% Triton X-100, 6% normal donkey serum (NDS; Jackson ImmunoResearch), and incubated overnight at 4°C with constant agitation in PBS with 0.2% Triton X-100, 2% NDS and chicken anti-TH monoclonal antibody (1:1000, Abcam, ab76442). Sections were then rinsed in PBS for 1 hour and incubated for 2 hours at room temperature with Alexa Fluor 488 goat anti-chicken antibody (1:1000, Life Technologies, UK) and DAPI (1:1000, Santa Cruz, USA). After subsequent rinses in PBS, sections were mounted on slides using Fluoromount Aqueous Mounting Medium (Sigma, UK) and visualised using a Leica SP5 confocal laser scanning microscope. Images were analysed using Fiji and the particle analyser plug-in. For each animal, 3 sections were selected for analysis containing rostral, middle and caudal parts of the VTA. For each section, three parts were imaged containing dorsal, middle and ventral parts of the parabrachial pigmented nucleus of the VTA. Each section was scanned with a 20x objective with 5x zoom, to produce a 5µm thick scan (z = 1µm). Total cells (TH and DAPI) were counted for each scan, an average computed for each section and then for each animal (i.e., 9 scans per animal), which was then expressed as a density based on the volume

of the scanned region. Immunohistochemistry and imaging were conducted blind to the experimental group.

2.6 | Behavioural testing

2.6.1 | Amphetamine-induced hyperlocomotion

Mice (*n* = 8 per genotype, 10-12 weeks old) were placed individually in the 40 x 40 x 40 cm black opaque Perspex XT open field arenas lit from below via infrared LED lighting for 30 minutes habituation. Following habituation, each mouse received an intraperitoneal (i.p.) injection of D-amphetamine (3mg kg^{-1}, Sigma-Aldrich), a dose that robustly induces hyperlocomotion in mice (Spielewoy et al., 2001; Papathanou et al., 2018). Mice were then placed back in the open field arenas and the distance moved was recorded for 60 minutes by an infrared camera (Sony) and Ethovision® XT software (Noldus, UK) for tracking spatial location of each mouse. The open field arena was cleaned and disinfected with Save4 odourless disinfectant (diluted 1:10) between each mouse.

2.6.2 | Sucrose preference test (SPT)

Before the test, each mouse (10-12 weeks old) was singly housed in an MB1 cage (NKP CAGES, overall size: 45 x 28 x 13 cm, internal size: 960 cm^2 x 13 cm). Mice were presented with identical bottles of water and the amount of water consumed for each was measured daily in order to determine the preferred bottle position. For the next two days, mice were adapted to sucrose by replacing the water bottle in the non-preferred position with an identical bottle containing 1 % (w/v) sucrose solution. The 1% sucrose solution was freshly prepared by dilution of sucrose (Fisher, Scientific UK) with tap water, and the amount of water and sucrose consumed was measured daily. Following an adaptation period (3 days), the sucrose preference test was performed. The position of the two bottles (water and 1% sucrose solution) was

randomly determined to avoid a place preference. The amount of sucrose solution and water consumed was measured daily (between 09:00 and 10:00) across three consecutive days and the % sucrose intake calculated.

2.7 | Statistics

All data are expressed as mean ± S.E.M. Shapiro-Wilk normality tests (supplementary Table 1) were undertaken for all data sets following which they were compared by paired or unpaired two-tailed Student's t-tests or two-tailed Mann-Whitney U non-parametric tests, one-way analysis of variance with Tukey's *post-hoc* correction or 2-way repeated-measures ANOVA followed by Bonferroni *post-hoc* correction as appropriate using GraphPad Prism (v5.0) or SigmaPlot (v12.0). Differences were considered significant when $p < 0.05$.

3 | Results

3.1 | Altered cerebral metabolism and regional functional connectivity in MKP-2$^{-/-}$ mice

LCGU was significantly and selectively increased in the VTA of MKP-2$^{-/-}$ mice (t(19)=2.103, p=0.049, n = 11, Figure 1a) when compared to MKP-2$^{+/+}$ control mice (n = 10). In all other (52) brain regions analysed, LCGU was not significantly altered in MKP-2$^{-/-}$ mice (Figure 1b & c, Table 1). The functional connectivity of the VTA to other brain regions was markedly altered in MKP-2$^{-/-}$ mice, with both increases and decreases in connectivity identified on a region-dependent basis (Figure 1b, Table 2). In this way, VTA connectivity to the nucleus accumbens shell (NacS), hippocampus (HC, dorsal hippocampus CA1 [DH-CA1] and ventral hippocampus dorsal subiculum [VH-DS]), the basolateral amygdala (BLA) and the median raphé (MR) was significantly reduced in MKP-2$^{-/-}$ mice. In contrast, the VTA showed increased functional connectivity to multiple components of the basal ganglia (ventromedial striatum [VMST], substantia nigra pars compacta [SNC] and the globus pallidus [GP]), and to the prelimbic cortex (PrL) in MKP-2$^{-/-}$ mice compared to MKP-2$^{+/+}$ mice (Figure 1b, Table 2).

3.2 | Increased sEPSC frequency onto VTA DA neurons in MKP-2$^{-/-}$ mice but neuronal excitability is unaltered.

Based on the increased glucose uptake in the VTA of MKP-2$^{-/-}$ mice and our previous results from the hippocampus (Abdul Rahman et al., 2016), we examined whether increased excitatory synaptic transmission onto dopamine neurons is increased in MKP-2$^{-/-}$ mice. Thus, we examined neuronal excitability and synaptic transmission of VTA DA neurons in acute brain slices, with neuronal identity of all I_H positive neurons confirmed post-experiment by co-localisation of biocytin with TH (Figure 2a). I_H amplitude was unaltered in VTA DA neurons (I_H at -100 mV: MKP-2$^{+/+}$, 118.3 ± 18.4 pA, *n* = 6; MKP-2$^{-/-}$, 114.7 ± 28.4 pA, n = 6; Figure

2b-d) as was the number of action potentials fired (200pA current injection: MKP-$2^{+/+}$, 5.3 ± 1.7, n = 4; MKP-$2^{-/-}$, 4.5 ± 2.2, n = 4; t(6) = 0.268, p = 0.797) and input resistance (-100pA current injection: MKP-$2^{+/+}$: 572.5 ± 70.4 MΩ, n = 4; MKP-$2^{-/-}$: 621.0 ± 117.6 MΩ, n = 4; t(6) = 0.356, p = 0.736) suggesting that the intrinsic firing properties of DA neurons in MKP-$2^{-/-}$ mice are unaltered. However, there was a significant increase in the frequency (MKP-$2^{+/+}$, 0.1 ± 0.1 Hz, n = 6; MKP-$2^{-/-}$, 0.7 ± 0.2 Hz, n = 6; U = 5, p = 0.044; Figure 2g) but not amplitude (MKP-$2^{+/+}$, 13.7 ± 1.1 pA, n = 6; MKP-$2^{-/-}$, 14.3 ± 1.4 pA, n = 6; t(10) = 0.366, p = 0.722; Figure 2h) of sEPSCs onto VTA DA neurons in MKP-$2^{-/-}$ slices when compared with MKP-$2^{+/+}$ controls.

3.3 | Changes in VTA neuronal density do not underlie altered functional connectivity.

Having established altered cerebral metabolism and region-specific alterations in functional connectivity in MKP-$2^{-/-}$ mice compared to MKP-$2^{+/+}$ controls, we next conducted immunohistochemistry using DAPI (a marker for cell nuclei) to examine cell density within the VTA. In addition, and given the prominent role of DA neurons in VTA function (Nair-Roberts et al., 2008; Creed et al., 2014; Walsh and Han, 2014), we also examined TH (the rate limiting enzyme in dopamine synthesis) to determine whether changes in the VTA neuronal density might be responsible for these findings in LCGU. Immunofluorescence indicated that the density of dopaminergic neurons (n = 6 for each genotype; t(10) = 0.957, p = 0.361), the density of all nuclei (n = 6 for each genotype; t(10) = 0.815, p = 0.434) and the ratio of dopaminergic neurons to all nuclei (n = 6 for each genotype; t(10) = 1.311, p = 0.219) in the VTA were unaltered in MKP-$2^{-/-}$ mice compared to MKP-$2^{+/+}$ control mice (Figure 3a, b). These results indicate that observed changes in VTA functional connectivity are unlikely to be due to differences in total cell number or the number of dopamine neurons.

3.4 | MKP-2 deletion alters reward processing.

Having established increased VTA function and altered connectivity in MKP-2$^{-/-}$ mice, we analysed their performance in relevant behavioural tests to determine if behaviours underpinned by these neural systems were altered. To investigate the function of the meso-corticolimbic dopamine system, we evaluated the behavioural sensitivity of MKP-2$^{-/-}$ mice to amphetamine (3mg kg^{-1}, i.p.). Consistent with our previous findings (Abdul Rahman et al., 2016), the general locomotor activity in MKP-2$^{-/-}$ mice was unaffected compared to MKP-2$^{+/+}$ control mice ($F_{(1,14)}$ = 0.080, p = 0.782, n=8 for both genotypes, Figure 4a). However, the amphetamine-induced hyperlocomotor response was significantly attenuated in MKP-2$^{-/-}$ compared to MKP-2$^{+/+}$ control mice ($F_{(1,14)}$ = 7.435, p = 0.016, n=8 for both genotypes, Figure 4a). We further investigated whether sucrose preference, a measure of reward processing and hedonic state, was altered in MKP-2$^{-/-}$ mice. Over a 3-day testing period, sucrose intake in MKP-2$^{-/-}$ mice was significantly increased on days 2 and 3 in MKP-2$^{-/-}$ mice compared to MKP-2$^{+/+}$ control mice (genotype effect: $F_{(1,28)}$ = 8.385, p = 0.007; no effect of time: $F_{(2,28)}$ = 2.158, p = 0.125, no interaction: $F_{(2,28)}$ = 0.256, p = 0.772; n=16 for both genotypes, Figure 4b).

4 | DISCUSSION

In the present study, we used an unbiased whole brain approach using MKP-2$^{-/-}$ mice to assess how MKP-2 deficiency impacts on brain function. We found that MKP-2 deletion results in a selective increase in VTA metabolism, as evidenced by local glucose utilisation, and altered functional connectivity of the VTA to diverse neural systems. Guided by these data, we undertook targeted characterisation of the VTA in MKP2$^{-/-}$ mice. We found that MKP-2 deletion did not alter VTA neuronal density or the intrinsic electrophysiological properties of VTA DA neurons, but increased glutamatergic synaptic activity onto VTA DA neurons was evident. Furthermore, we confirmed that MKP-2$^{-/-}$ mice exhibited behavioural deficits relevant to the VTA dysfunction identified, including reduced amphetamine-induced hyperlocomotion and increased sucrose preference.

4.1 | Increased VTA metabolism and functional connectivity in MKP-2$^{-/-}$ mice.

^{14}C-2-DG autoradiographic imaging has been used to identify localised changes in brain metabolism in numerous studies (Dawson et al., 2012, 2013). Recently, studies have utilised mathematical algorithms to investigate alterations in connectivity between brain regions using ^{14}C-2-DG data (Dawson et al., 2012, 2013, 2015). As MAPK pathways have diverse roles within the CNS, we examined whether MKP-2 deletion led to alterations in metabolism in discrete brain regions and disrupted functional brain connectivity. Our ^{14}C-2-DG data indicates that LCGU is significantly and selectively increased in the VTA of MKP-2$^{-/-}$ mice and that its functional connectivity is altered in a region-specific manner. This includes altered functional connectivity between the VTA and subfields of the prefrontal cortex, striatum, and the hippocampus (Figure 1, Tables 1 & 2), which is consistent with our previous observation of altered hippocampal-dependent spatial learning in these mice (Abdul Rahman et al., 2016). The mesolimbic system is established as an essential component of the reward system with the VTA

and NAc playing critical roles in reward processing (Cohen et al., 2012; Creed and Lüscher, 2013), with altered reward processing being associated with alterations in MAPK activity (Jia et al., 2013; Ciccarelli and Giustetto, 2014). Given our understanding of VTA function and our observations regarding increased VTA metabolism and altered functional connectivity in MKP-2$^{-/-}$ mice, we hypothesised that these alterations would lead to changes in relevant behavioural tests, including tests characterising reward processing.

4.2 | sEPSC frequency onto VTA dopaminergic neurons is increased in MKP-2$^{-/-}$ mice.

Having established that MKP-2 deletion leads to changes in VTA metabolism and functional connectivity, we next examined the alterations in VTA neuronal excitability and synaptic activity underlying these observations. An increase in sEPSC frequency, but not amplitude, onto I_H positive VTA neurons in MKP-2$^{-/-}$ mice was observed, indicating that presynaptic functional changes result in enhanced glutamate release. This increased excitatory drive may contribute to the increased VTA metabolism observed in these mice. However, the exact mechanisms that underlie this increased sEPSC frequency remain elusive. One possibility is that ERK activity is increased presynaptically in the absence of MKP-2, which would lead to changes in presynaptic release machinery and/or the number of docked vesicles (Kushner, 2005; Giachello et al., 2010). This finding may account for the increased sEPSC frequency observed in the present study. However, given that ERK activity has previously been shown to be unaltered in MKP-2$^{-/-}$ mice when examined in tissue from various brain regions (Abdul Rahman et al., 2016), whether presynaptically localised changes in ERK activity in the VTA accounts for this remains unknown. To date ERK activity in synapses onto VTA neurons has not yet been characterised in MKP-2$^{-/-}$ mice, so the possibility of a selective increase in this region remains a possibility that certainly warrants further investigation. Additionally, it should also be noted that whilst the VTA contains a heterogeneous population of neuronal types

including dopaminergic, GABAergic and glutamatergic neurons (Nair-Roberts et al., 2008; Creed et al., 2014; Morales and Root, 2014; Walsh and Han, 2014), here we have focussed on glutamatergic synaptic activity onto VTA DA neurons. Hence, it would be interesting to characterise the synaptic activity onto other identified neuronal subtypes within the VTA. Strikingly, increased synaptic connectivity in the VTA is observed following injections of rewarding drugs of abuse (Ungless et al., 2001; Oliva and Wanat, 2016; Francis et al., 2018), with these drug-induced increases in synaptic strength being primarily mediated by postsynaptic changes. In contrast, the classic interpretation of our findings in relation to increased sEPSC frequency but not amplitude, are that these changes are mediated presynaptically. This suggestion is also consistent with the observation that ^{14}C-2-DG and glucose metabolism largely reflects local synaptic activity in the brain region of interest. However, it would be interesting to further characterise the functional basis of the increased sEPSCs seen in the VTA of MKP2$^{-/-}$ mice using paired pulse facilitation and AMPA/NMDA ratio paradigms in order to identify the exact locus of increased sEPSC frequency.

4.3 | Altered VTA function is not due to structural changes in MKP-2$^{-/-}$ mice.

Having established that MKP-2 deletion leads to changes in VTA function, we examined whether structural changes within the VTA accounted for these observations. We found that the density of dopaminergic neurons, the density of all nuclei, and the ratio of dopaminergic neurons to all nuclei were not altered in MKP-2$^{-/-}$ mice, indicating that VTA structural changes do not underlie our observations of altered VTA metabolism and functional connectivity in these animals. This raises the question as to the nature of the physiological changes within the VTA that underlie our observations, and generally rules out the contribution of gross cellular neurodevelopmental alterations as the primary mechanism underlying VTA dysfunction in MKP-2$^{-/-}$ mice. However, at present it is still unclear as to whether altered VTA metabolism

and connectivity in MKP-2$^{-/-}$ mice is mediated by more subtle development effects, for example through effects on neuronal differentiation (Kim et al., 2015), or whether the effect of a lifelong loss of MKP-2 function can be reversed by acutely rescuing VTA MKP-2 function in these animals. While our observation that VTA dopaminergic neuronal density is not altered in MKP-2$^{-/-}$ mice is suggestive that reduced VTA LCGU is not mediated by developmental proliferation defects, at least for DA neurons, this potential mechanism requires further investigation and the impact on other neuronal cell types still remains as a plausible contributory mechanism.

4.4 | Impaired amphetamine-induced locomotor activity but increased sucrose preference in MKP-2$^{-/-}$ mice.

Since it is well established that rewarding drugs of abuse modulate synaptic transmission and plasticity onto the dopaminergic VTA neurons (Ungless et al., 2001; Oliva and Wanat, 2016; Francis et al., 2018) and we observed synaptic dysfunction in the VTA of these animals, we investigated the effect of amphetamine injection in MKP-2$^{-/-}$ mice using the open field test. Surprisingly, locomotor activity was decreased in MKP-2$^{-/-}$ mice injected with amphetamine compared with that observed in MKP-2$^{+/+}$ mice. There is much debate regarding the brain regions and mechanisms involved in psychostimulant-induced behaviour and addiction but altered VTA connectivity is strongly implicated (Hyman and Malenka, 2001; Morales and Margolis, 2017). In particular, it is well established that psychostimulant drugs, including amphetamine, result in increased extracellular DA levels that contribute to the resultant hyperlocomotion (Heshmati and Russo, 2015; Morales and Margolis, 2017). Indeed, recent studies have proposed a key role for VGLUT2 containing VTA DA neuronal connectivity with the NAc in psychostimulant-induced behaviour and hyperlocomotion (Birgner et al., 2010; Hnasko et al., 2010; Fortin et al., 2012; Papathanou et al., 2018). The similarity between these

findings and our own in regard to impaired response to amphetamine and the reduced VTA-NAc functional connectivity seen in MKP-2$^{-/-}$ mice is intriguing and warrants further work.

To examine whether the mesolimbic system dysfunction seen in MKP-2$^{-/-}$ mice results in alterations in reward processing, we used the sucrose preference test, an established method for investigating hedonic state. Consistent with an increase in VTA LCGU metabolism, MKP-2$^{-/-}$ mice displayed a greater preference for sucrose than MKP-2$^{+/+}$ mice. In agreement with our findings, previous studies have revealed that optogenetic inhibition of VTA dopaminergic neurons leads to decreased sucrose preference in mice (Cohen et al., 2012; Nieh et al., 2015). Furthermore, increased VTA activity is associated with increased reward seeking behaviour (Kempadoo et al., 2013; Creed et al., 2014) and our observations of altered hippocampal-VTA-accumbens functional connectivity in MKP-2$^{-/-}$ mice are consistent with the established role of this neural circuit in reward processing and novelty detection (Lisman and Grace, 2005; Morales and Margolis, 2017). Hence, this may also contribute to the altered sucrose preference seen in these animals. Intriguingly, these data suggest that the decreased expression of MKP-2 seen in the brains of patients with depression (Dwivedi et al., 2001) and schizophrenia (Kyosseva et al., 1999), may contribute to the anhedonia seen in these disorders, which may be mediated, in part, by the influence of MKP-2 on the VTA and mesolimbic reward system function. Clearly, further studies are required to elucidate the potential role of MKP-2 dysfunction in the aetiology of these disorders and MKP-2's potential contribution to altered reward processing and motivation.

Our data reveal contrasting results between increased preference for the natural reward of sucrose compared to the drug-induced effects of amphetamine. Whilst a clear rationale for this is unknown, it is generally accepted that amphetamine-induced hyperlocomotion is a selective

challenge of the dopaminergic system and reflects increased DA levels in mesolimbic regions, whereas sucrose preference is proposed to engage several neuronal circuits/systems (Heshmati and Russo, 2015; Morales and Margolis, 2017). These contrasting results could be examined further through targeted deletion of VTA MKP-2 in wild-type mice that would allow normal development and the determination of the acute effects of MKP-2 signalling, or via targeted MKP-2 reintroduction into the VTA of MKP-2$^{-/-}$ mice in order to rescue the phenotypes observed here. However, these experiments are clearly beyond the scope if this initial unbiased whole brain approach.

Taken together, the present study reveals a novel role for MKP-2 in reward processing paralleled by concomitant changes in VTA function and functional connectivity. These findings indicate that MKP-2 may play role in the altered reward processing that occurs in CNS disorders associated with MKP-2 dysfunction, particularly those in which altered reward processing is prominent.

ACKNOWLEDGEMENTS

K.P. and N.D. contributed equally to this work. K.P. was funded by "Mobility Plus" Program (1661/MOB/V/2017/0), Ministry of Science and Higher Education, Poland. The immunohistochemical research was supported by grant MC-A654-5QB70 from the U.K. Medical Research Council (MRC) to M.A.U.

COMPETING INTERESTS

The authors declare no competing interests.

AUTHOR CONTRIBUTIONS

K.P., N.D., M.A.U. and T.J.B. designed research; K.P., N.D., K.T., M.A.U., R.R.B. and T.J.B. performed research; K.P., N.D., K.T., M.A.U., R.R.B. and T.J.B. analyzed data; all authors contributed to the writing of the paper.

DATA ACCESSIBILITY

Primary data are available from the authors on request.

References

Abdul Rahman, N. Z., Greenwood, S. M., Brett, R. R., Tossell, .K, Ungless, M. A., Plevin, R. & Bushell, T.J. (2016) Mitogen-activated protein kinase phosphatase-2 deletion impairs synaptic plasticity and hippocampal-dependent memory. J. Neurosci., **36,** 2348–2354.

Al-Mutairi, M. S., Cadalbert, L. C., McGachy, H. A., Shweash, M., Schroeder, J., Kurnik, M., Sloss, C.M., Bryant, C.E., Alexander, J. & Plevin, R. (2010) MAP kinase phosphatase-2 plays a critical role in response to infection by Leishmania mexicana. PLoS Pathog., **6,** 1–11.

Barthas, F., Humo, M., Gilsbach, R., Waltisperger, E., Karatas, M., Leman, S., Hein, L., Belzung, C., Boutillier, A-L, Barrot, M. & Yalcin I (2017) Cingulate overexpression of mitogen-activated protein kinase phosphatase-1 as a key factor for depression. Biol. Psychiatry, **82,** 370–379.

Birgner, C., Nordenankar, K., Lundblad, M., Mendez, J. A., Smith, C., le Grevès, M., Galter, D., Olson, L., Fredriksson, A., Trudeau, L-E, Kullander, K. & Wallén-Mackenzie, A. (2010) VGLUT2 in dopamine neurons is required for psychostimulant-induced behavioral activation. Proc. Natl. Acad. Sci. USA, **107,** 389–394.

Caunt, C. J. & Keyse, S. M. (2013)Dual-specificity MAP kinase phosphatases (MKPs): shaping
the outcome of MAP kinase signalling. FEBS J., **280,** 489-504.

Chen, Y., Wang, H., Zhang, R., Wang, H., Peng, Z., Sun, R. & Tan, Q. (2012) Microinjection of sanguinarine into the ventrolateral orbital cortex inhibits Mkp-1 and exerts an antidepressant-like effect in rats. Neurosci. Lett., **506,** 327–331.

Ciccarelli, A. & Giustetto, M. (2014) Role of ERK signaling in activity-dependent modifications of histone proteins. Neuropharmacology **80,** 34–44.

Cohen, J. Y., Haesler, S., Vong, L., Lowell, B.B. & Uchida, N. (2012) Neuron-type-specific signals for reward and punishment in the ventral tegmental area. Nature, **482,** 85–88.

Creed, M. C. & Lüscher, C. (2013) Drug-evoked synaptic plasticity: beyond metaplasticity. Curr. Opin. Neurobiol., **23,** 553–558.

Creed MC, Ntamati NR, Tan KR (2014) VTA GABA neurons modulate specific learning behaviors through the control of dopamine and cholinergic systems. Front. Behav. Neurosci., **8**, 8.

Dawson, N., Ferrington, L., Lesch, K-P. & Kelly, P. A. T. (2011). Cerebral metabolic responses to 5-HT2A/C receptor activation in mice with gneetically modified serotonin transporter (SERT) expression. European Neuropharmacology, **21,** 117-128.

Dawson, N., Thompson, R. J., McVie, A., Thomson, D. M., Morris, B. J. & Pratt JA (2012) Modafinil reverses phencyclidine-induced deficits in cognitive flexibility, cerebral metabolism, and functional brain connectivity. Schizophr. Bull., **38,** 457–474.

Dawson, N., Morris, B. J. & Pratt, J. A. (2013) Subanaesthetic ketamine treatment alters prefrontal cortex connectivity with thalamus and ascending subcortical systems. Schizophr. Bull., **39,** 366–377.

Dawson, N., Kurihara, M., Thomson, D. M., Winchester, C.L., McVie, A., Hedde, J. R., Randall, A. D., Shen, S., Seymour, P.A., Hughes, Z. A., Dunlop, J., Brown, J. T., Brandon, N. J., Morris, B. J. & Pratt, J.A. (2015) Altered functional brain network connectivity and glutamate system function in transgenic mice expressing truncated Disrupted-in-Schizophrenia 1. Transl. Psychiatry, **5,** e569–e569.

Duric, V., Banasr, M., Licznerski, P., Schmidt, H. D., Stockmeier, C. A., Simen, A. A., Newton, S. S. & Duman, R. S. (2010) A negative regulator of MAP kinase causes depressive behavior. Nat. Med., **16,** 1328–1332.

Dwivedi, Y., Rizavi, H. S., Roberts, R. C., Conley, R. C., Tamminga, C. A. & Pandey, G.N. (2001) Reduced activation and expression of ERK1/2 MAP kinase in the post-mortem brain of depressed suicide subjects. J. Neurochem., **77,** 916–928.

Fortin, G. M., Bourque, M-J., Mendez, J. A., Leo, D., Nordenankar, K., Birgner, C., Arvidsson, E., Rymar, V. V., Bérubé-Carrière, N., Claveau, A-M., Descarries, L., Sadikot, A. F., Wallén-Mackenzie, A. & Trudeau, L-E. (2012) Glutamate corelease promotes growth and survival of midbrain dopamine neurons. J. Neurosci., **32,** 17477–17491.

Francis, T. C., Gantz, S. C., Moussawi, K. & Bonci, A. (2018) Synaptic and intrinsic plasticity in the ventral tegmental area after chronic cocaine. Curr. Opin. Neurobiol., **54,** 66–72.

Giachello, C. N. G., Fiumara, F., Giacomini, C., Corradi, A., Milanese, C., Ghirardi, M., Benfenati, F. & Montarolo, P. G. (2010) MAPK/Erk-dependent phosphorylation of synapsin mediates formation of functional synapses and short-term homosynaptic plasticity. J. Cell. Sci., **123,** 881–893.

Heshmati, M. & Russo, S.J. (2015) Anhedonia and the brain reward circuitry in depression. Curr Behav. Neurosci. Rep., **2,** 146–153.

Hnasko, T. S., Chuhma, N., Zhang, H., Goh, G. Y., Sulzer, D., Palmiter, R. D., Rayport, S. & Edwards, R. H. (2010) Vesicular glutamate transport promotes dopamine storage and glutamate corelease in vivo. Neuron, **65,** 643–656.

Hughes, R., Whittingham-Dowd, J., Simmons, R., Clapcote, S., Broughton, S. J. & Dawson N. (2019) Ketamine restores thalamic-prefrontal cortex functional connecitivity in a mouse model of neurodevelopmental disorder-associated 2p16.3 deletion. Cerebral Cortex, doi: 10.1093/cercor/bhz44.

Hui, L-Y., Wang, Y-W., Zhou, F-L., Ma, X-C., Yan, R-Z., Zhang, L., Wang, Q-L. & Yu. X. (2016) Association between MKP-1, BDNF, and gonadal hormones with depression on perimenopausal women. J. Womens Health, **25,** 71–77.

Hyman, S. E. &, Malenka, R.C. (2001) Addiction and the brain: the neurobiology of compulsion and its persistence. Nat. Rev. Neurosci., **2,** 695–703.

Jeanneteau, F., Deinhardt, K., Miyoshi, G., Bennett, A. M. & Chao, M. V. (2010) The MAP kinase phosphatase MKP-1 regulates BDNF-induced axon branching. Nat. Neurosci., **13,** 1373–1379.

Jia, W., Liu, R., Shi, J., Wu, B., Dang, W., Du, Y., Zhou, Q., Wang, J. & Zhang, R. (2013) Differential regulation of MAPK phosphorylation in the dorsal hippocampus in response to prolonged morphine withdrawal-induced depressive-like symptoms in mice. PLoS ONE, **8,** e66111.

Kempadoo, K. A., Tourino, C., Cho, S. L., Magnani, F., Leinninger, G-M., Stuber, G. D., Zhang, F., Myers, M. G., Deisseroth, K., de Lecea, L. & Bonci, A. (2013) Hypothalamic neurotensin projections promote reward by enhancing glutamate transmission in the VTA. J. Neurosci., **33,** 7618–7626.

Keshet, Y. & Seger, R. (2010) The MAP Kinase Signaling Cascades: A System of Hundreds of Components Regulates a Diverse Array of Physiological Functions. In: Neurotrophic Factors (Skaper SD, ed), pp 3–38 Methods in Molecular Biology. Totowa, NJ: Humana Press.

Kim, S.Y., Han, Y-M., Oh, M., Kim, W-K., Oh, K-J., Lee, S. C. Bae, K-H. & Han, B-S. (2015) DUSP4 regulates neuronal differentiation and calcium homeostasis by modulating ERK1/2 phosphorylation. Stem Cells Dev., **24,** 686–700.

Kushner, S. A. (2005) Modulation of presynaptic plasticity and learning by the H-ras/extracellular signal-regulated kinase/synapsin I signaling pathway. J. Neurosci., **25,** 9721–9734.

Kyosseva, S. V., Elbein, A. D., Griffin, W. S., Mrak, R. E., Lyon, M. & Karson, C. N. (1999) Mitogen-activated protein kinases in schizophrenia. Biol. Psychiatry, **46,** 689–696.

Lee, J. K. & Kim, N. J. (2017) Recent Advances in the Inhibition of p38 MAPK as a Potential Strategy for the Treatment of Alzheimer's Disease. Molecules, 22.

Lisman, J. E. & Grace, A. A. (2005) The hippocampal-VTA loop: controlling the entry of information into long-term memory. Neuron, **46,** 703–713.

Marshall, C. J. (1995) Specificity of receptor tyrosine kinase signaling: transient versus sustained extracellular signal-regulated kinase activation. Cell, **80,** 179–185.

Mevik B.-H. & Wehrens R. (2007) The pls package: principle component and partial least squares regression in R. J Stat Software, **18,** 1-23.

Morales, M. & Margolis, E. B. (2017) Ventral tegmental area: cellular heterogeneity, connectivity and behaviour. Nat. Rev. Neurosci., **18,** 73–85.

Morales, M. & Root, D. H. (2014) Glutamate neurons within the midbrain dopamine regions. Neuroscience, **282,** 60–68.

Nair-Roberts, R. G., Chatelain-Badie, S. D., Benson, E., White-Cooper, H., Bolam, J. P., Ungless, M. A. (2008) Stereological estimates of dopaminergic, GABAergic and glutamatergic neurons in the ventral tegmental area, substantia nigra and retrorubral field in the rat. Neuroscience, **152,** 1024–1031.

Nieh, E. H., Matthews, G. A., Allsop, S. A., Presbrey, K. N., Leppla, C. A., Wichmann, R., Neve, R., Wildes, C. P. & Tye, K. M. (2015) Decoding neural circuits that control compulsive sucrose seeking. Cell, **160,** 528–541.

Oliva, I. & Wanat, M. J (2016) Ventral tegmental area afferents and drug-dependent behaviors. Front Psychiatry **7,** 30.

Papathanou, M., Creed, M., Dorst, M. C., Bimpisidis, Z. , Dumas, S., Pettersson, H., Bellone, C., Silberberg, G., Lüscher, C. & Wallén-Mackenzie, A. (2018) Targeting VGLUT2 in mature dopamine neurons decreases mesoaccumbal glutamatergic transmission and identifies a role for glutamate co-release in synaptic plasticity by increasing baseline AMPA/NMDA ratio. Front. Neural Circuits, **12,** 64.

R Core Team (2018). R: A language and environment for statistical computing. R Foundation for Statistical Computing, Vienna, Austria. URL https://www.R-project.org./

Samuels, I. S., Saitta, S. C. & Landreth, G. E. (2009) MAP'ing CNS development and cognition: an ERKsome process. Neuron, **61,** 160–167.

Sokoloff, L., Reivich, M., Kennedy, C., Des Rosiers, M. H., Patlak, C. S., Pettigrew, K. D., Sakurada, O. & Shinohara, M. (1977) The [14C]Deoxyglucose method for the measurement of

local cerebral glucose utilisation: theory, procedure and normal values in the conscious anethetized albino rat. J. Neurochem., **28,** 897-916.

Spielewoy, C., Biala, G., Roubert, C., Hamon, M., Betancur, C. & Giros, B. (2001) Hypolocomotor effects of acute and daily d-amphetamine in mice lacking the dopamine transporter. Psychopharmacology, **159,** 2–9.

Thomas, G. M. & Huganir, R. L. (2004) MAPK cascade signalling and synaptic plasticity. Nat. Rev. Neurosci., **5,** 173–183.

Ungless, M. A., Whistler, J. L., Malenka, R. C. & Bonci, A. (2001) Single cocaine exposure in vivo induces long-term potentiation in dopamine neurons. Nature, **411,** 583–587.

Vithayathil, J., Pucilowska, J. & Landreth, G. E. (2018) ERK/MAPK signaling and autism spectrum disorders. Prog. Brain Res., **241,** 63-112.

Walsh, J. J. & Han, M. H. (2014) The heterogeneity of ventral tegmental area neurons: Projection functions in a mood-related context. Neuroscience, **282C,** 101–108.

Yasuda, S., Sugiura, H., Tanaka, H., Takigami, S. & Yamagata, K. (2011) p38 MAP kinase inhibitors as potential therapeutic drugs for neural diseases. Cent. Nerv. Syst. Agents Med. Chem., **11,** 45–59.

Figure Captions

Figure 1. Altered VTA metabolism and functional connectivity in MKP-2$^{-/-}$ mice. (a) LCGU is selectively increased in the VTA of MKP-2$^{-/-}$ mice (n = 11) compared to MKP-2$^{+/+}$ control mice (n = 10) but not in (b) the ventral hippocampal CA1 region or (c) the central amygdala. (d-i) Summary statistical diagrams showing altered VTA functional connectivity in MKP-2$^{-/-}$ mice. Brain section figures are modified from the Allen mouse brain atlas (http://mouse.brain-map.org/static/atlas). Blue denotes regions that have significantly lost functional connectivity with the VTA in MKP-2$^{-/-}$ mice. Red denotes regions that show significantly gained functional connectivity to the VTA in MKP-2$^{-/-}$ but not MKP-2$^{+/+}$ mice. Yellow highlights the anatomical localisation of the VTA. (j) The functional connectivity heatmap also shows the lost (blue) and gained (red) alterations in VTA functional connectivity in MKP2-/- mice. Amyg. = Amygdala, Dorsal Hip.= Dorsal Hippocampus, Ventral Hip.= Ventral Hippocampus, Aud. = Auditory System, Multi.= Mutlimodal regions. Regional abbreviations and their systems are shown in Table 1. Differences in LCGU between groups was analysed using unpaired two-tailed Student's t-test with * $p < 0.05$ vs MKP-2$^{+/+}$ controls. Full LCGU and functional connectivity data are shown in Tables 1 and 2 respectively.

Figure 2. Increased sEPSC frequency onto VTA DA neurons in MKP-2$^{-/-}$ mice. (a) Representative images and traces of co-localisation of biocytin (magenta) filled I_H positive neuron and tyrosine hydroxylase (TH; green) in the VTA. (b-c) Representative I_H traces recorded from MKP-2$^{+/+}$ and MKP-2$^{-/-}$ VTA neurons respectively. (d) I_H amplitude is unaffected in VTA DA neurons from MKP-2$^{-/-}$ mice when compared to MKP-2$^{+/+}$ controls (n = 6). (e-f) Representative sEPSC traces from MKP$^{+/+}$ and MKP$^{-/-}$ mice respectively. (g) sEPSC frequency is increased in MKP-2$^{-/-}$ slices (n = 6) compared to MKP$^{+/+}$ slices (n = 6) whereas (h) sEPSC amplitude is unchanged. Data were analysed using 2-way repeated-measures ANOVA followed

by Bonferroni *post-hoc* correction (I_H) and two-tailed Mann-Whitney U non-parametric tests (sEPSCs) with * $p < 0.05$ *vs* MKP-$2^{+/+}$ controls. N is equal to one neuron per slice per animal with all I_H positive neurons confirmed to be DA neurons (TH positive) post experiment.

Figure 3. No change in dopamine neuron number in MKP-$2^{-/-}$ mice. (**a)** Immunostaining for tyrosine hydroxylase (TH; green) and DAPI (blue) appeared normal in MKP-$2^{-/-}$ mice (n = 6) compared to MKP-$2^{+/+}$ control mice (n=6). (b) Quantitative analyses revealed no significant differences between the densities of dopaminergic (TH+ve) neurons, total cell bodies (DAPI) and the ratio of TH / total cells in MKP-$2^{-/-}$ mice compared to MKP-$2^{+/+}$ control mice. Data analysed using unpaired two-tailed Student's t-tests.

Figure 4. Reduced amphetamine-induced hyperlocomotion but increased sucrose preference in MKP-$2^{-/-}$ mice. (a) Amphetamine (3mg kg^{-1}, i.p.)-induced hyperlocomotion is significantly attenuated in MKP-$2^{-/-}$ mice (n=8 for both genotypes). (b) Sucrose intake (1% solution) in relation to total fluid intake is significantly increased in MKP-$2^{-/-}$ mice compared to MKP-$2^{+/+}$ mice on trial days 2 and 3 (n=16 for both genotypes). Both sets of data were analysed using 2-way repeated-measures ANOVA followed by Bonferroni *post-hoc* correction with * $p < 0.05$ *vs* MKP-$2^{+/+}$ controls.

Mitogen-activated protein kinase phosphatase-2 deletion modifies ventral tegmental area function and connectivity and alters reward processing.

Karolina Pytka[1,2], Neil Dawson[1,3], Kyoko Tossell[4,5], Mark A. Ungless[4,5], Robin Plevin[1], Ros R. Brett[1] and Trevor J. Bushell[1*]

[1] Strathclyde Institute of Pharmacy & Biomedical Sciences, University of Strathclyde, 161 Cathedral Street, Glasgow, G4 0RE, UK,

[2] Department of Pharmacodynamics, Faculty of Pharmacy, Jagiellonian University Medical College, Medyczna 9, 30-688 Krakow, Poland,

[3] Division of Biomedical and Life Sciences, Lancaster University, Lancaster, LA1 4YQ, UK,

[4] MRC London Institute of Medical Sciences (LMS), Du Cane Road, London W12 0NN, UK

[5] Institute of Clinical Sciences (ICS), Faculty of Medicine, Imperial College London, Du Cane Road, London W12 0NN, UK

*Corresponding author:

T.J. Bushell, Strathclyde Institute of Pharmacy & Biomedical Sciences, University of Strathclyde, 161 Cathedral Street, Glasgow G4 0RE, UK. Tel: 0141 548 2856, Fax: 0141 552 2562, Email: trevor.bushell@strath.ac.uk

Running title: MKP-2 deletion alters VTA function and connectivity.

Number of pages: 31 Number of figures: 4 Number of tables: 2 Supplementary table: 1

Number of words: i) whole manuscript 7577 ii) Abstract: 219.

Keywords: mitogen-activated protein kinase phosphatase-2, local cerebral glucose utilization, spontaneous excitatory postsynaptic current, sucrose preference, amphetamine-induced hyperlocomotion.

K.P. and N.D. contributed equally to this work.

ABSTRACT

Mitogen-activated protein kinases (MAPKs) regulate normal brain functioning and their dysfunction is implicated in a number of brain disorders. Thus, there is great interest in understanding the signalling systems that control MAPK functioning. One family of proteins that contribute to this process, the mitogen-activated protein kinase phosphatases (MKPs), directly inactivate MAPKs through dephosphorylation. Recent studies have identified novel functions of MKPs in foetal development, the immune system, cancer and synaptic plasticity and memory. In the present study, we performed an unbiased investigation using MKP-2$^{-/-}$ mice to assess whether MKP-2 plays a global role in modulating brain function. Local cerebral glucose utilization is significantly increased in the ventral tegmental area (VTA) of MKP-2$^{-/-}$ mice, with connectivity analysis revealing alterations in VTA functional connectivity, including a significant reduction in connectivity to the nucleus accumbens and hippocampus. In addition, spontaneous excitatory postsynaptic current frequency, but not amplitude, onto putative dopamine neurons in the VTA is increased in MKP-2$^{-/-}$ mice, which indicates that increased excitatory drive may account for the increased VTA glucose utilization. Consistent with modified VTA function and connectivity, in behavioural tests MKP-2$^{-/-}$ mice exhibited increased sucrose preference and impaired amphetamine-induced hyperlocomotion. Overall, these data reveal that MKP-2 plays a role in modulating VTA function and that its dysfunction may contribute to brain disorders in which altered reward processing is present.

ABBREVIATIONS

^{14}C-2-DG - ^{14}C-2-deoxyglucose

ACSF - artificial cerebrospinal fluid

BDNF - brain-derived neurotrophic factor

BSA - bovine serum albumin

CNS - central nervous system

DA - dopamine

DUSP - dual-specificity phosphatases

ERK - extracellular signal related kinase

FBS - fetal bovine serum

JNK - c-jun N-terminal kinase

LCGU - local cerebral glucose utilization

MAPK - mitogen-activated protein kinase

MKP - mitogen-activated protein kinase phosphatase

NDS – normal donkey serum

PLSR - partial least squares regression algorithm

PBS - phosphate-buffered saline

PFA - paraformaldehyde

RoI - region of interest

sEPSC - spontaneous excitatory postsynaptic current

SPT - sucrose preference test

TH - tyrosine hydroxylase

VIP - variable importance to the projection

VTA - ventral tegmental area

1 | INTRODUCTION

The mitogen-activated protein kinases (MAPK) form a family of evolutionally conserved proteins, which play a critical role in various cellular processes including cellular proliferation, differentiation, development, transformation and apoptosis (Keshet and Seger, 2010). The mammalian MAPK family consists of the extracellular signal related kinase (ERK), the c-jun N-terminal kinase (JNK) and p38 MAPK. MAPK signalling shares a common three-tiered core structure, where the activation of MAPK requires sequential phosphorylation and activation of each component kinase. The activated MAPKs then convert the extracellular stimuli into a broad range of cellular responses. In the central nervous system (CNS), MAPKs are expressed in numerous cell types, where they play a role in the regulation of synaptic transmission and plasticity (Thomas and Huganir, 2004; Samuels *et al.,* 2009). In addition, their dysfunction has been implicated in CNS disorders including Alzheimer's disease, autism, Parkinson's disease, anxiety and addiction (Yasuda et al., 2011; Lee & Kim, 2017; Vithayathil et al., 2018).

The duration and magnitude of MAPK activation are crucial in determining the physiological outcome of this signalling pathway (Marshall, 1995; Caunt & Keyse, 2013). Thus, the negative regulation of phosphorylation process is vital for controlling MAPK signalling. The process of MAPK inactivation is mediated by the family of dual-specificity phosphatases (DUSPs), the mitogen-activated protein kinase phosphatases (MKPs), which catalyse the dephosphorylation of MAPK that consequently leads to inhibiting their activity. However, our knowledge of MKP function in the CNS is limited but studies suggest a role for the prototypic *Dusp1* (MKP-1) in brain-derived neurotrophic factor (BDNF)-induced axonal branching (Jeanneteau *et al*., 2010) and depression (Duric et al., 2010; Chen et al., 2012; Jia et al., 2013; Hui et al., 2016; Barthas et al., 2017). In contrast, the role of *Dusp4* (MKP-2) in the CNS has not been studied extensively. However, we have recently shown that *Dusp4* deletion increases hippocampal

spontaneous excitatory postsynaptic potential (sEPSC) frequency as well as impairing spatial reference and working memory (Abdul Rahman et al., 2016).

Building on our previous findings and given our limited knowledge of MKP-2 function in the CNS, we performed an unbiased investigation using MKP-2$^{-/-}$ mice to examine the consequence of *Dusp4* gene deletion on brain function and behaviour.

2 | MATERIALS AND METHODS

2.1 | Animals

All *in vivo* experimental procedures were in accordance with UK legislation (Animals (Scientific Procedures) Act 1986) and with approval by the University of Strathclyde Ethics Committee. All experiments were completed using male MKP-$2^{+/+}$ and MKP-$2^{-/-}$ mice generated as previously described (Al-Mutairi et al., 2010), normally group-housed (5–6 per cage) under standard conditions (21°C, 45%–65% humidity, 12h dark/light cycle [lights on 06:00]) in cages provided with environmental enrichment in the form of a plastic refuge and nesting material. Animals had free access to food and water with all behavioural procedures carried out between 09.00 and 17.00. Mice were randomly assigned to the treatment groups with the experimenter blinded to each group.

2.2 | ^{14}C-2-Deoxyglucose (^{14}C-2-DG) functional brain imaging

Local cerebral glucose utilization (LCGU) was determined in MKP-$2^{-/-}$ (n = 11) and MKP- $2^{+/+}$ (n = 10) mice (10-12 weeks old) in accordance with previously published protocols , using an approach adapted from the original protocol developed in rats (Sokoloff et al., 1977) for application in conscious freely-moving mice (Dawson et al., 2011, 2013). In brief, LCGU measurement was initiated by injection of ^{14}C-2-DG (*intraperitoneally* (*i.p.*), 4.625 MBq/kg in physiological saline at 2.5ml/kg (Perkin-Elmer, UK) and animals were returned to their home cage. Forty five minutes after ^{14}C-2-DG injection animals were decapitated and a terminal blood sample collected, by torso inversion, into heparinized weigh boats. Plasma glucose concentrations (mmol/L) were detected from whole blood using a blood glucose monitor (Accu-Chek Aviva). The brain was then rapidly dissected out intact, frozen in isopentane (-40°C) and stored at (-80°C) until sectioning. Blood samples were centrifuged to isolate plasma, and plasma ^{14}C concentrations (20µl) were determine by liquid scintillation analysis (Packard).

Frozen brains were sectioned (20µm) in the coronal plane in a cryostat (-20°C). A series of three consecutive sections were retained from every 60µm, thaw mounted onto slide covers and rapidly dried on a hotplate (70°C). Autoradiograms were generated by apposing these sections, together with precalibrated ^{14}C standards (39-1098 nCi/g tissue equivalents, Amersham International, UK) to x-ray film (Carestream BioMax MR film, Sigma-Aldrich, UK) for 7 days. Autoradiographic images were analysed by a computer based image analysis system (MCID/M5+, Interfocus, UK). The local isotope concentration for each brain region of interest (RoI) was derived from the optical density of the autoradiographic images relative to that of the coexposed ^{14}C standards, with 8-12 replicate measurements taken per RoI in each animal. LCGU was determined in 53 anatomically distinct brain RoI as the ratio of ^{14}C present in that region relative to the average ^{14}C-2-DG concentration in the whole brain of the same animal, referred to as the ^{14}C-2-DG uptake ratio. There was no significant difference between the whole brain average ^{14}C-2-DG concentration in MKP-2$^{-/-}$ mice relative to wild-type controls (MKP-2$^{+/+}$ 142.05 ± 7.74 nCi/g; MKP-2$^{-/-}$ 164.80 ± 8.27 nCi/g, p=0.103 Student's t-test), suggesting that MKP-2 deletion did not significantly impact global cerebral metabolism. In addition, there was no significant difference in plasma ^{14}C-2-DG levels (MKP-2$^{+/+}$ 22.9 ± 1.58 nCi/ml, MKP-2$^{-/-}$ 29.21 ± 3.33 nCi/ml, p=0.115 Student's t-test) or glucose levels (MKP-2$^{+/+}$ 9.00 ± 0.35 mmol/L, MKP-2$^{-/-}$ 8.28 ± 0.46 mmol/L, p=0.224 Student's t-test) between the two experimental groups, suggesting that there were no systematic difference in plasma glucose or ^{14}C-2-DG concentrations between the two experimental groups that might impact on LCGU measurement.

2.3 | Functional brain connectivity analysis using PLSR

The partial least squares regression algorithm (PLSR) was employed to define significant differences in the functional connectivity of selected "seed" RoI to all other RoI analysed from the functional ^{14}C-2-DG brain imaging data, as previously outlined (Dawson et al., 2012, 2013;

Hughes et al., 2019), and was undertaken using the PLS package (Mevik and Wehrens, 2007) in R (R Core Team, 2018). The analysed "seed" brain RoI were those regions in which a significant alteration in overt LCGU was observed, namely the ventral tegmental area (VTA, Figure 1). In brief, functional connectivity between the "seed" RoI and all other RoI analysed was defined by the variable importance to the projection (VIP) statistic gained from the PLSR models. A region was considered to be functionally connected to the "seed" region if the 95% confidence interval (95% CI) of the VIP statistic exceeded 0.8. This denotes a considerable contribution of the explanatory variable (RoI metabolism) to the dependent variable ("seed" RoI metabolism) in PLSR models. The standard deviation (SD) and 95% CI of the VIP statistic were estimated by jack-knifing. Significant differences in the VIP statistic between groups were analysed using t-test with Bonferroni *post-hoc* correction for multiple comparisons on the basis of the number of potentially connected RoI (52). Thus genotype-induced alterations in regional functional connectivity to the VTA were defined in terms of lost (VIP 95% CI >0.8 in MKP-$2^{+/+}$ mice, VIP 95% CI <0.8 in MKP-$2^{+/-}$ mice and $p<0.05$ significant difference between genotypes) and abnormally gained (VIP 95% CI <0.8 in MKP-$2^{+/+}$ mice, VIP 95% CI >0.8 in MKP-$2^{+/-}$ mice and $p<0.05$ significant difference between genotypes) connectivity in MKP-$2^{-/-}$ mice.

2.4 | Electrophysiology

Mice (19–25 days old) were killed by cervical dislocation and decapitated. The brains were rapidly removed and placed immediately in an ice-cold (0–3°C), oxygenated (95% O_2/5% CO_2) artificial cerebrospinal fluid (ACSF) containing (in mM): 124 NaCl, 3 KCl, 26 $NaHCO_3$, 2.5 NaH_2PO_4, 2 $MgSO_4$, 2 $CaCl_2$, 10 glucose. Horizontal slices (230 μm) were cut using a vibratome and transferred to a holding chamber containing oxygenated ACSF, equilibrated at 37°C for 30 min followed for 30 min at the room temperature prior to recording. Slices were

then transferred into a submerged recording chamber continuously perfused with ACSF at a flow rate at 2-3 mL min^{-1} at room temperature. Electrodes (4-7 MΩ) were filled with an internal solution containing (in mM): 130 $KMeSO_4$, 20 KCl, 4 Mg-ATP, 0.4 Na-GTP, 0.5 EGTA, 10 HEPES, 0.5% (w/v) biocytin, pH 7.2, 290 mOsm. Visually-guided whole-cell patch-clamp recordings were made from neurons in the VTA using an Axopatch 200B amplifier (Molecular Devices, USA), connected to a personal computer interfaced with Digidata 1322A interface (Molecular Devices, USA) and captured using pClamp9.0 software (Molecular Devices, USA). Spontaneous EPSCs were recorded at -70mV for 5 min periods, digitized at 5kHz. For I_H recordings, cells were held at -70mV in voltage clamp mode with -10mV increments at 10s intervals. Data were analysed offline using pClamp9.2 software (Molecular Devices, USA) or MiniAnalysis software (Synaptosoft, USA). For all slice experiments, n is equal to one neuron per slice per animal with all I_H positive neurons confirmed to be dopaminergic (DAergic) neurons post experiment using immunohistochemistry (see below).

2.5 | Immunohistochemistry

2.5.1 | Confirmation of VTA dopamine (DA) neuron identity

Immediately following electrophysiological experiments, each slice was fixed in 4% paraformaldehyde (PFA) for 1 h, then washed with phosphate-buffered saline (PBS). Slices were then agitated in PBS with 1% Triton X-100 for 1 h. Free-floating slices were then pre-blocked for 1 h at room temperature in PBS with 0.5% Triton X-100, 1% (w/v) bovine serum albumin (BSA) and 5% (v/v) fetal bovine serum (FBS) and incubated overnight at 4°C with chicken polyclonal anti-tyrosine hydroxylase (TH) antibody (1:500, Abcam, ab76442) with 0.5% Triton X-100, 1% (w/v) BSA and 5% (v/v) FBS. Slices were rinsed in PBS and incubated for 3 h with goat anti-chicken Alexa Fluor™ 555 (1:200, Life Technologies, A21437) and streptavidin-Alexa Fluor™ 488 (1: 500, Life Technologies, S11223) with 0.5% Triton X-100,

1% (w/v) BSA and 5% (v/v) FBS. After subsequent PBS rinses, slices were mounted on slides using Vectashield anti-fade mounting medium with DAPI (Vector Laboratories) and visualized using a Leica SP5 confocal laser-scanning microscope.

2.5.2 | VTA structure

Male MKP-2$^{-/-}$ and MKP-2$^{+/+}$ mice (10-12 weeks old, n=6 for both genotypes) were perfused transcardially with 4% PFA. Brains were removed and post-fixed for 1 hour in 4% PFA, washed with PBS, followed by cryoprotection in 30% sucrose. Coronal brain sections (70µm) were prepared using a cryostat (Leica). Slices were rinsed with PBS and agitated in PBS with 0.5% Triton X-100 for 15 min. Free-floating sections were then pre-blocked for 1 hour at room temperature in PBS with 0.2% Triton X-100, 6% normal donkey serum (NDS; Jackson ImmunoResearch), and incubated overnight at 4°C with constant agitation in PBS with 0.2% Triton X-100, 2% NDS and chicken anti-TH monoclonal antibody (1:1000, Abcam, ab76442). Sections were then rinsed in PBS for 1 hour and incubated for 2 hours at room temperature with Alexa Fluor 488 goat anti-chicken antibody (1:1000, Life Technologies, UK) and DAPI (1:1000, Santa Cruz, USA). After subsequent rinses in PBS, sections were mounted on slides using Fluoromount Aqueous Mounting Medium (Sigma, UK) and visualised using a Leica SP5 confocal laser scanning microscope. Images were analysed using Fiji and the particle analyser plug-in. For each animal, 3 sections were selected for analysis containing rostral, middle and caudal parts of the VTA. For each section, three parts were imaged containing dorsal, middle and ventral parts of the parabrachial pigmented nucleus of the VTA. Each section was scanned with a 20x objective with 5x zoom, to produce a 5µm thick scan (z = 1µm). Total cells (TH and DAPI) were counted for each scan, an average computed for each section and then for each animal (i.e., 9 scans per animal), which was then expressed as a density based on the volume

of the scanned region. Immunohistochemistry and imaging were conducted blind to the experimental group.

2.6 | Behavioural testing

2.6.1 | Amphetamine-induced hyperlocomotion

Mice (*n* = 8 per genotype, 10-12 weeks old) were placed individually in the 40 x 40 x 40 cm black opaque Perspex XT open field arenas lit from below via infrared LED lighting for 30 minutes habituation. Following habituation, each mouse received an intraperitoneal (i.p.) injection of D-amphetamine (3mg kg^{-1}, Sigma-Aldrich), a dose that robustly induces hyperlocomotion in mice (Spielewoy et al., 2001; Papathanou et al., 2018). Mice were then placed back in the open field arenas and the distance moved was recorded for 60 minutes by an infrared camera (Sony) and Ethovision® XT software (Noldus, UK) for tracking spatial location of each mouse. The open field arena was cleaned and disinfected with Save4 odourless disinfectant (diluted 1:10) between each mouse.

2.6.2 | Sucrose preference test (SPT)

Before the test, each mouse (10-12 weeks old) was singly housed in an MB1 cage (NKP CAGES, overall size: 45 x 28 x 13 cm, internal size: 960 cm^2 x 13 cm). Mice were presented with identical bottles of water and the amount of water consumed for each was measured daily in order to determine the preferred bottle position. For the next two days, mice were adapted to sucrose by replacing the water bottle in the non-preferred position with an identical bottle containing 1 % (w/v) sucrose solution. The 1% sucrose solution was freshly prepared by dilution of sucrose (Fisher, Scientific UK) with tap water, and the amount of water and sucrose consumed was measured daily. Following an adaptation period (3 days), the sucrose preference test was performed. The position of the two bottles (water and 1% sucrose solution) was

randomly determined to avoid a place preference. The amount of sucrose solution and water consumed was measured daily (between 09:00 and 10:00) across three consecutive days and the % sucrose intake calculated.

2.7 | Statistics

All data are expressed as mean ± S.E.M. Shapiro-Wilk normality tests (supplementary Table 1) were undertaken for all data sets following which they were compared by paired or unpaired two-tailed Student's t-tests or two-tailed Mann-Whitney U non-parametric tests, one-way analysis of variance with Tukey's *post-hoc* correction or 2-way repeated-measures ANOVA followed by Bonferroni *post-hoc* correction as appropriate using GraphPad Prism (v5.0) or SigmaPlot (v12.0). Differences were considered significant when $p < 0.05$.

3 | Results

3.1 | Altered cerebral metabolism and regional functional connectivity in MKP-2$^{-/-}$ mice

LCGU was significantly and selectively increased in the VTA of MKP-2$^{-/-}$ mice (t(19)=2.103, p=0.049, n = 11, Figure 1a) when compared to MKP-2$^{+/+}$ control mice (n = 10). In all other (52) brain regions analysed, LCGU was not significantly altered in MKP-2$^{-/-}$ mice (Figure 1b & c, Table 1). The functional connectivity of the VTA to other brain regions was markedly altered in MKP-2$^{-/-}$ mice, with both increases and decreases in connectivity identified on a region-dependent basis (Figure 1b, Table 2). In this way, VTA connectivity to the nucleus accumbens shell (NacS), hippocampus (HC, dorsal hippocampus CA1 [DH-CA1] and ventral hippocampus dorsal subiculum [VH-DS]), the basolateral amygdala (BLA) and the median raphé (MR) was significantly reduced in MKP-2$^{-/-}$ mice. In contrast, the VTA showed increased functional connectivity to multiple components of the basal ganglia (ventromedial striatum [VMST], substantia nigra pars compacta [SNC] and the globus pallidus [GP]), and to the prelimbic cortex (PrL) in MKP-2$^{-/-}$ mice compared to MKP-2$^{+/+}$ mice (Figure 1b, Table 2).

3.2 | Increased sEPSC frequency onto VTA DA neurons in MKP-2$^{-/-}$ mice but neuronal excitability is unaltered.

Based on the increased glucose uptake in the VTA of MKP-2$^{-/-}$ mice and our previous results from the hippocampus (Abdul Rahman et al., 2016), we examined whether increased excitatory synaptic transmission onto dopamine neurons is increased in MKP-2$^{-/-}$ mice. Thus, we examined neuronal excitability and synaptic transmission of VTA DA neurons in acute brain slices, with neuronal identity of all I_H positive neurons confirmed post-experiment by co-localisation of biocytin with TH (Figure 2a). I_H amplitude was unaltered in VTA DA neurons (I_H at -100 mV: MKP-2$^{+/+}$, 118.3 ± 18.4 pA, *n* = 6; MKP-2$^{-/-}$, 114.7 ± 28.4 pA, n = 6; Figure

2b-d) as was the number of action potentials fired (200pA current injection: MKP-$2^{+/+}$, 5.3 ± 1.7, n = 4; MKP-$2^{-/-}$, 4.5 ± 2.2, n = 4; t(6) = 0.268, p = 0.797) and input resistance (-100pA current injection: MKP-$2^{+/+}$: 572.5 ± 70.4 MΩ, n = 4; MKP-$2^{-/-}$: 621.0 ± 117.6 MΩ, n = 4; t(6) = 0.356, p = 0.736) suggesting that the intrinsic firing properties of DA neurons in MKP-$2^{-/-}$ mice are unaltered. However, there was a significant increase in the frequency (MKP-$2^{+/+}$, 0.1 ± 0.1 Hz, n = 6; MKP-$2^{-/-}$, 0.7 ± 0.2 Hz, n = 6; U = 5, p = 0.044; Figure 2g) but not amplitude (MKP-$2^{+/+}$, 13.7 ± 1.1 pA, n = 6; MKP-$2^{-/-}$, 14.3 ± 1.4 pA, n = 6; t(10) = 0.366, p = 0.722; Figure 2h) of sEPSCs onto VTA DA neurons in MKP-$2^{-/-}$ slices when compared with MKP-$2^{+/+}$ controls.

3.3 | Changes in VTA neuronal density do not underlie altered functional connectivity.

Having established altered cerebral metabolism and region-specific alterations in functional connectivity in MKP-$2^{-/-}$ mice compared to MKP-$2^{+/+}$ controls, we next conducted immunohistochemistry using DAPI (a marker for cell nuclei) to examine cell density within the VTA. In addition, and given the prominent role of DA neurons in VTA function (Nair-Roberts et al., 2008; Creed et al., 2014; Walsh and Han, 2014), we also examined TH (the rate limiting enzyme in dopamine synthesis) to determine whether changes in the VTA neuronal density might be responsible for these findings in LCGU. Immunofluorescence indicated that the density of dopaminergic neurons (n = 6 for each genotype; t(10) = 0.957, p = 0.361), the density of all nuclei (n = 6 for each genotype; t(10) = 0.815, p = 0.434) and the ratio of dopaminergic neurons to all nuclei (n = 6 for each genotype; t(10) = 1.311, p = 0.219) in the VTA were unaltered in MKP-$2^{-/-}$ mice compared to MKP-$2^{+/+}$ control mice (Figure 3a, b). These results indicate that observed changes in VTA functional connectivity are unlikely to be due to differences in total cell number or the number of dopamine neurons.

3.4 | MKP-2 deletion alters reward processing.

Having established increased VTA function and altered connectivity in MKP-2$^{-/-}$ mice, we analysed their performance in relevant behavioural tests to determine if behaviours underpinned by these neural systems were altered. To investigate the function of the meso-corticolimbic dopamine system, we evaluated the behavioural sensitivity of MKP-2$^{-/-}$ mice to amphetamine (3mg kg^{-1}, i.p.). Consistent with our previous findings (Abdul Rahman et al., 2016), the general locomotor activity in MKP-2$^{-/-}$ mice was unaffected compared to MKP-2$^{+/+}$ control mice ($F_{(1,14)}$ = 0.080, p = 0.782, n=8 for both genotypes, Figure 4a). However, the amphetamine-induced hyperlocomotor response was significantly attenuated in MKP-2$^{-/-}$ compared to MKP-2$^{+/+}$ control mice ($F_{(1,14)}$ = 7.435, p = 0.016, n=8 for both genotypes, Figure 4a). We further investigated whether sucrose preference, a measure of reward processing and hedonic state, was altered in MKP-2$^{-/-}$ mice. Over a 3-day testing period, sucrose intake in MKP-2$^{-/-}$ mice was significantly increased on days 2 and 3 in MKP-2$^{-/-}$ mice compared to MKP-2$^{+/+}$ control mice (genotype effect: $F_{(1,28)}$ = 8.385, p = 0.007; no effect of time: $F_{(2,28)}$ = 2.158, p = 0.125, no interaction: $F_{(2,28)}$ = 0.256, p = 0.772; n=16 for both genotypes, Figure 4b).

4 | DISCUSSION

In the present study, we used an unbiased whole brain approach using MKP-2$^{-/-}$ mice to assess how MKP-2 deficiency impacts on brain function. We found that MKP-2 deletion results in a selective increase in VTA metabolism, as evidenced by local glucose utilisation, and altered functional connectivity of the VTA to diverse neural systems. Guided by these data, we undertook targeted characterisation of the VTA in MKP2$^{-/-}$ mice. We found that MKP-2 deletion did not alter VTA neuronal density or the intrinsic electrophysiological properties of VTA DA neurons, but increased glutamatergic synaptic activity onto VTA DA neurons was evident. Furthermore, we confirmed that MKP-2$^{-/-}$ mice exhibited behavioural deficits relevant to the VTA dysfunction identified, including reduced amphetamine-induced hyperlocomotion and increased sucrose preference.

4.1 | Increased VTA metabolism and functional connectivity in MKP-2$^{-/-}$ mice.

^{14}C-2-DG autoradiographic imaging has been used to identify localised changes in brain metabolism in numerous studies (Dawson et al., 2012, 2013). Recently, studies have utilised mathematical algorithms to investigate alterations in connectivity between brain regions using ^{14}C-2-DG data (Dawson et al., 2012, 2013, 2015). As MAPK pathways have diverse roles within the CNS, we examined whether MKP-2 deletion led to alterations in metabolism in discrete brain regions and disrupted functional brain connectivity. Our ^{14}C-2-DG data indicates that LCGU is significantly and selectively increased in the VTA of MKP-2$^{-/-}$ mice and that its functional connectivity is altered in a region-specific manner. This includes altered functional connectivity between the VTA and subfields of the prefrontal cortex, striatum, and the hippocampus (Figure 1, Tables 1 & 2), which is consistent with our previous observation of altered hippocampal-dependent spatial learning in these mice (Abdul Rahman et al., 2016). The mesolimbic system is established as an essential component of the reward system with the VTA

and NAc playing critical roles in reward processing (Cohen et al., 2012; Creed and Lüscher, 2013), with altered reward processing being associated with alterations in MAPK activity (Jia et al., 2013; Ciccarelli and Giustetto, 2014). Given our understanding of VTA function and our observations regarding increased VTA metabolism and altered functional connectivity in MKP-2$^{-/-}$ mice, we hypothesised that these alterations would lead to changes in relevant behavioural tests, including tests characterising reward processing.

4.2 | sEPSC frequency onto VTA dopaminergic neurons is increased in MKP-2$^{-/-}$ mice.

Having established that MKP-2 deletion leads to changes in VTA metabolism and functional connectivity, we next examined the alterations in VTA neuronal excitability and synaptic activity underlying these observations. An increase in sEPSC frequency, but not amplitude, onto I_H positive VTA neurons in MKP-2$^{-/-}$ mice was observed, indicating that presynaptic functional changes result in enhanced glutamate release. This increased excitatory drive may contribute to the increased VTA metabolism observed in these mice. However, the exact mechanisms that underlie this increased sEPSC frequency remain elusive. One possibility is that ERK activity is increased presynaptically in the absence of MKP-2, which would lead to changes in presynaptic release machinery and/or the number of docked vesicles (Kushner, 2005; Giachello et al., 2010). This finding may account for the increased sEPSC frequency observed in the present study. However, given that ERK activity has previously been shown to be unaltered in MKP-2$^{-/-}$ mice when examined in tissue from various brain regions (Abdul Rahman et al., 2016), whether presynaptically localised changes in ERK activity in the VTA accounts for this remains unknown. To date ERK activity in synapses onto VTA neurons has not yet been characterised in MKP-2$^{-/-}$ mice, so the possibility of a selective increase in this region remains a possibility that certainly warrants further investigation. Additionally, it should also be noted that whilst the VTA contains a heterogeneous population of neuronal types

including dopaminergic, GABAergic and glutamatergic neurons (Nair-Roberts et al., 2008; Creed et al., 2014; Morales and Root, 2014; Walsh and Han, 2014), here we have focussed on glutamatergic synaptic activity onto VTA DA neurons. Hence, it would be interesting to characterise the synaptic activity onto other identified neuronal subtypes within the VTA. Strikingly, increased synaptic connectivity in the VTA is observed following injections of rewarding drugs of abuse (Ungless et al., 2001; Oliva and Wanat, 2016; Francis et al., 2018), with these drug-induced increases in synaptic strength being primarily mediated by postsynaptic changes. In contrast, the classic interpretation of our findings in relation to increased sEPSC frequency but not amplitude, are that these changes are mediated presynaptically. This suggestion is also consistent with the observation that ^{14}C-2-DG and glucose metabolism largely reflects local synaptic activity in the brain region of interest. However, it would be interesting to further characterise the functional basis of the increased sEPSCs seen in the VTA of MKP2$^{-/-}$ mice using paired pulse facilitation and AMPA/NMDA ratio paradigms in order to identify the exact locus of increased sEPSC frequency.

4.3 | Altered VTA function is not due to structural changes in MKP-2$^{-/-}$ mice.

Having established that MKP-2 deletion leads to changes in VTA function, we examined whether structural changes within the VTA accounted for these observations. We found that the density of dopaminergic neurons, the density of all nuclei, and the ratio of dopaminergic neurons to all nuclei were not altered in MKP-2$^{-/-}$ mice, indicating that VTA structural changes do not underlie our observations of altered VTA metabolism and functional connectivity in these animals. This raises the question as to the nature of the physiological changes within the VTA that underlie our observations, and generally rules out the contribution of gross cellular neurodevelopmental alterations as the primary mechanism underlying VTA dysfunction in MKP-2$^{-/-}$ mice. However, at present it is still unclear as to whether altered VTA metabolism

and connectivity in MKP-2$^{-/-}$ mice is mediated by more subtle development effects, for example through effects on neuronal differentiation (Kim et al., 2015), or whether the effect of a lifelong loss of MKP-2 function can be reversed by acutely rescuing VTA MKP-2 function in these animals. While our observation that VTA dopaminergic neuronal density is not altered in MKP-2$^{-/-}$ mice is suggestive that reduced VTA LCGU is not mediated by developmental proliferation defects, at least for DA neurons, this potential mechanism requires further investigation and the impact on other neuronal cell types still remains as a plausible contributory mechanism.

4.4 | Impaired amphetamine-induced locomotor activity but increased sucrose preference in MKP-2$^{-/-}$ mice.

Since it is well established that rewarding drugs of abuse modulate synaptic transmission and plasticity onto the dopaminergic VTA neurons (Ungless et al., 2001; Oliva and Wanat, 2016; Francis et al., 2018) and we observed synaptic dysfunction in the VTA of these animals, we investigated the effect of amphetamine injection in MKP-2$^{-/-}$ mice using the open field test. Surprisingly, locomotor activity was decreased in MKP-2$^{-/-}$ mice injected with amphetamine compared with that observed in MKP-2$^{+/+}$ mice. There is much debate regarding the brain regions and mechanisms involved in psychostimulant-induced behaviour and addiction but altered VTA connectivity is strongly implicated (Hyman and Malenka, 2001; Morales and Margolis, 2017). In particular, it is well established that psychostimulant drugs, including amphetamine, result in increased extracellular DA levels that contribute to the resultant hyperlocomotion (Heshmati and Russo, 2015; Morales and Margolis, 2017). Indeed, recent studies have proposed a key role for VGLUT2 containing VTA DA neuronal connectivity with the NAc in psychostimulant-induced behaviour and hyperlocomotion (Birgner et al., 2010; Hnasko et al., 2010; Fortin et al., 2012; Papathanou et al., 2018). The similarity between these

findings and our own in regard to impaired response to amphetamine and the reduced VTA-NAc functional connectivity seen in MKP-2$^{-/-}$ mice is intriguing and warrants further work.

To examine whether the mesolimbic system dysfunction seen in MKP-2$^{-/-}$ mice results in alterations in reward processing, we used the sucrose preference test, an established method for investigating hedonic state. Consistent with an increase in VTA LCGU metabolism, MKP-2$^{-/-}$ mice displayed a greater preference for sucrose than MKP-2$^{+/+}$ mice. In agreement with our findings, previous studies have revealed that optogenetic inhibition of VTA dopaminergic neurons leads to decreased sucrose preference in mice (Cohen et al., 2012; Nieh et al., 2015). Furthermore, increased VTA activity is associated with increased reward seeking behaviour (Kempadoo et al., 2013; Creed et al., 2014) and our observations of altered hippocampal-VTA-accumbens functional connectivity in MKP-2$^{-/-}$ mice are consistent with the established role of this neural circuit in reward processing and novelty detection (Lisman and Grace, 2005; Morales and Margolis, 2017). Hence, this may also contribute to the altered sucrose preference seen in these animals. Intriguingly, these data suggest that the decreased expression of MKP-2 seen in the brains of patients with depression (Dwivedi et al., 2001) and schizophrenia (Kyosseva et al., 1999), may contribute to the anhedonia seen in these disorders, which may be mediated, in part, by the influence of MKP-2 on the VTA and mesolimbic reward system function. Clearly, further studies are required to elucidate the potential role of MKP-2 dysfunction in the aetiology of these disorders and MKP-2's potential contribution to altered reward processing and motivation.

Our data reveal contrasting results between increased preference for the natural reward of sucrose compared to the drug-induced effects of amphetamine. Whilst a clear rationale for this is unknown, it is generally accepted that amphetamine-induced hyperlocomotion is a selective

challenge of the dopaminergic system and reflects increased DA levels in mesolimbic regions, whereas sucrose preference is proposed to engage several neuronal circuits/systems (Heshmati and Russo, 2015; Morales and Margolis, 2017). These contrasting results could be examined further through targeted deletion of VTA MKP-2 in wild-type mice that would allow normal development and the determination of the acute effects of MKP-2 signalling, or via targeted MKP-2 reintroduction into the VTA of MKP-2$^{-/-}$ mice in order to rescue the phenotypes observed here. However, these experiments are clearly beyond the scope if this initial unbiased whole brain approach.

Taken together, the present study reveals a novel role for MKP-2 in reward processing paralleled by concomitant changes in VTA function and functional connectivity. These findings indicate that MKP-2 may play role in the altered reward processing that occurs in CNS disorders associated with MKP-2 dysfunction, particularly those in which altered reward processing is prominent.

ACKNOWLEDGEMENTS

K.P. and N.D. contributed equally to this work. K.P. was funded by "Mobility Plus" Program (1661/MOB/V/2017/0), Ministry of Science and Higher Education, Poland. The immunohistochemical research was supported by grant MC-A654-5QB70 from the U.K. Medical Research Council (MRC) to M.A.U.

COMPETING INTERESTS

The authors declare no competing interests.

AUTHOR CONTRIBUTIONS

K.P., N.D., M.A.U. and T.J.B. designed research; K.P., N.D., K.T., M.A.U., R.R.B. and T.J.B. performed research; K.P., N.D., K.T., M.A.U., R.R.B. and T.J.B. analyzed data; all authors contributed to the writing of the paper.

DATA ACCESSIBILITY

Primary data are available from the authors on request.

References

Abdul Rahman, N. Z., Greenwood, S. M., Brett, R. R., Tossell, .K, Ungless, M. A., Plevin, R. & Bushell, T.J. (2016) Mitogen-activated protein kinase phosphatase-2 deletion impairs synaptic plasticity and hippocampal-dependent memory. J. Neurosci., **36,** 2348–2354.

Al-Mutairi, M. S., Cadalbert, L. C., McGachy, H. A., Shweash, M., Schroeder, J., Kurnik, M., Sloss, C.M., Bryant, C.E., Alexander, J. & Plevin, R. (2010) MAP kinase phosphatase-2 plays a critical role in response to infection by Leishmania mexicana. PLoS Pathog., **6,** 1–11.

Barthas, F., Humo, M., Gilsbach, R., Waltisperger, E., Karatas, M., Leman, S., Hein, L., Belzung, C., Boutillier, A-L, Barrot, M. & Yalcin I (2017) Cingulate overexpression of mitogen-activated protein kinase phosphatase-1 as a key factor for depression. Biol. Psychiatry, **82,** 370–379.

Birgner, C., Nordenankar, K., Lundblad, M., Mendez, J. A., Smith, C., le Grevès, M., Galter, D., Olson, L., Fredriksson, A., Trudeau, L-E, Kullander, K. & Wallén-Mackenzie, A. (2010) VGLUT2 in dopamine neurons is required for psychostimulant-induced behavioral activation. Proc. Natl. Acad. Sci. USA, **107,** 389–394.

Caunt, C. J. & Keyse, S. M. (2013)Dual-specificity MAP kinase phosphatases (MKPs): shaping
the outcome of MAP kinase signalling. FEBS J., **280,** 489-504.

Chen, Y., Wang, H., Zhang, R., Wang, H., Peng, Z., Sun, R. & Tan, Q. (2012) Microinjection of sanguinarine into the ventrolateral orbital cortex inhibits Mkp-1 and exerts an antidepressant-like effect in rats. Neurosci. Lett., **506,** 327–331.

Ciccarelli, A. & Giustetto, M. (2014) Role of ERK signaling in activity-dependent modifications of histone proteins. Neuropharmacology **80,** 34–44.

Cohen, J. Y., Haesler, S., Vong, L., Lowell, B.B. & Uchida, N. (2012) Neuron-type-specific signals for reward and punishment in the ventral tegmental area. Nature, **482,** 85–88.

Creed, M. C. & Lüscher, C. (2013) Drug-evoked synaptic plasticity: beyond metaplasticity. Curr. Opin. Neurobiol., **23,** 553–558.

Creed MC, Ntamati NR, Tan KR (2014) VTA GABA neurons modulate specific learning behaviors through the control of dopamine and cholinergic systems. Front. Behav. Neurosci., **8**, 8.

Dawson, N., Ferrington, L., Lesch, K-P. & Kelly, P. A. T. (2011). Cerebral metabolic responses to 5-HT2A/C receptor activation in mice with gneetically modified serotonin transporter (SERT) expression. European Neuropharmacology, **21,** 117-128.

Dawson, N., Thompson, R. J., McVie, A., Thomson, D. M., Morris, B. J. & Pratt JA (2012) Modafinil reverses phencyclidine-induced deficits in cognitive flexibility, cerebral metabolism, and functional brain connectivity. Schizophr. Bull., **38,** 457–474.

Dawson, N., Morris, B. J. & Pratt, J. A. (2013) Subanaesthetic ketamine treatment alters prefrontal cortex connectivity with thalamus and ascending subcortical systems. Schizophr. Bull., **39,** 366–377.

Dawson, N., Kurihara, M., Thomson, D. M., Winchester, C.L., McVie, A., Hedde, J. R., Randall, A. D., Shen, S., Seymour, P.A., Hughes, Z. A., Dunlop, J., Brown, J. T., Brandon, N. J., Morris, B. J. & Pratt, J.A. (2015) Altered functional brain network connectivity and glutamate system function in transgenic mice expressing truncated Disrupted-in-Schizophrenia 1. Transl. Psychiatry, **5,** e569–e569.

Duric, V., Banasr, M., Licznerski, P., Schmidt, H. D., Stockmeier, C. A., Simen, A. A., Newton, S. S. & Duman, R. S. (2010) A negative regulator of MAP kinase causes depressive behavior. Nat. Med., **16,** 1328–1332.

Dwivedi, Y., Rizavi, H. S., Roberts, R. C., Conley, R. C., Tamminga, C. A. & Pandey, G.N. (2001) Reduced activation and expression of ERK1/2 MAP kinase in the post-mortem brain of depressed suicide subjects. J. Neurochem., **77,** 916–928.

Fortin, G. M., Bourque, M-J., Mendez, J. A., Leo, D., Nordenankar, K., Birgner, C., Arvidsson, E., Rymar, V. V., Bérubé-Carrière, N., Claveau, A-M., Descarries, L., Sadikot, A. F., Wallén-Mackenzie, A. & Trudeau, L-E. (2012) Glutamate corelease promotes growth and survival of midbrain dopamine neurons. J. Neurosci., **32,** 17477–17491.

Francis, T. C., Gantz, S. C., Moussawi, K. & Bonci, A. (2018) Synaptic and intrinsic plasticity in the ventral tegmental area after chronic cocaine. Curr. Opin. Neurobiol., **54,** 66–72.

Giachello, C. N. G., Fiumara, F., Giacomini, C., Corradi, A., Milanese, C., Ghirardi, M., Benfenati, F. & Montarolo, P. G. (2010) MAPK/Erk-dependent phosphorylation of synapsin mediates formation of functional synapses and short-term homosynaptic plasticity. J. Cell. Sci., **123,** 881–893.

Heshmati, M. & Russo, S.J. (2015) Anhedonia and the brain reward circuitry in depression. Curr Behav. Neurosci. Rep., **2,** 146–153.

Hnasko, T. S., Chuhma, N., Zhang, H., Goh, G. Y., Sulzer, D., Palmiter, R. D., Rayport, S. & Edwards, R. H. (2010) Vesicular glutamate transport promotes dopamine storage and glutamate corelease in vivo. Neuron, **65,** 643–656.

Hughes, R., Whittingham-Dowd, J., Simmons, R., Clapcote, S., Broughton, S. J. & Dawson N. (2019) Ketamine restores thalamic-prefrontal cortex functional connecitivity in a mouse model of neurodevelopmental disorder-associated 2p16.3 deletion. Cerebral Cortex, doi: 10.1093/cercor/bhz44.

Hui, L-Y., Wang, Y-W., Zhou, F-L., Ma, X-C., Yan, R-Z., Zhang, L., Wang, Q-L. & Yu. X. (2016) Association between MKP-1, BDNF, and gonadal hormones with depression on perimenopausal women. J. Womens Health, **25,** 71–77.

Hyman, S. E. &, Malenka, R.C. (2001) Addiction and the brain: the neurobiology of compulsion and its persistence. Nat. Rev. Neurosci., **2,** 695–703.

Jeanneteau, F., Deinhardt, K., Miyoshi, G., Bennett, A. M. & Chao, M. V. (2010) The MAP kinase phosphatase MKP-1 regulates BDNF-induced axon branching. Nat. Neurosci., **13,** 1373–1379.

Jia, W., Liu, R., Shi, J., Wu, B., Dang, W., Du, Y., Zhou, Q., Wang, J. & Zhang, R. (2013) Differential regulation of MAPK phosphorylation in the dorsal hippocampus in response to prolonged morphine withdrawal-induced depressive-like symptoms in mice. PLoS ONE, **8,** e66111.

Kempadoo, K. A., Tourino, C., Cho, S. L., Magnani, F., Leinninger, G-M., Stuber, G. D., Zhang, F., Myers, M. G., Deisseroth, K., de Lecea, L. & Bonci, A. (2013) Hypothalamic neurotensin projections promote reward by enhancing glutamate transmission in the VTA. J. Neurosci., **33,** 7618–7626.

Keshet, Y. & Seger, R. (2010) The MAP Kinase Signaling Cascades: A System of Hundreds of Components Regulates a Diverse Array of Physiological Functions. In: Neurotrophic Factors (Skaper SD, ed), pp 3–38 Methods in Molecular Biology. Totowa, NJ: Humana Press.

Kim, S.Y., Han, Y-M., Oh, M., Kim, W-K., Oh, K-J., Lee, S. C. Bae, K-H. & Han, B-S. (2015) DUSP4 regulates neuronal differentiation and calcium homeostasis by modulating ERK1/2 phosphorylation. Stem Cells Dev., **24,** 686–700.

Kushner, S. A. (2005) Modulation of presynaptic plasticity and learning by the H-ras/extracellular signal-regulated kinase/synapsin I signaling pathway. J. Neurosci., **25,** 9721–9734.

Kyosseva, S. V., Elbein, A. D., Griffin, W. S., Mrak, R. E., Lyon, M. & Karson, C. N. (1999) Mitogen-activated protein kinases in schizophrenia. Biol. Psychiatry, **46,** 689–696.

Lee, J. K. & Kim, N. J. (2017) Recent Advances in the Inhibition of p38 MAPK as a Potential Strategy for the Treatment of Alzheimer's Disease. Molecules, 22.

Lisman, J. E. & Grace, A. A. (2005) The hippocampal-VTA loop: controlling the entry of information into long-term memory. Neuron, **46,** 703–713.

Marshall, C. J. (1995) Specificity of receptor tyrosine kinase signaling: transient versus sustained extracellular signal-regulated kinase activation. Cell, **80,** 179–185.

Mevik B.-H. & Wehrens R. (2007) The pls package: principle component and partial least squares regression in R. J Stat Software, **18,** 1-23.

Morales, M. & Margolis, E. B. (2017) Ventral tegmental area: cellular heterogeneity, connectivity and behaviour. Nat. Rev. Neurosci., **18,** 73–85.

Morales, M. & Root, D. H. (2014) Glutamate neurons within the midbrain dopamine regions. Neuroscience, **282,** 60–68.

Nair-Roberts, R. G., Chatelain-Badie, S. D., Benson, E., White-Cooper, H., Bolam, J. P., Ungless, M. A. (2008) Stereological estimates of dopaminergic, GABAergic and glutamatergic neurons in the ventral tegmental area, substantia nigra and retrorubral field in the rat. Neuroscience, **152,** 1024–1031.

Nieh, E. H., Matthews, G. A., Allsop, S. A., Presbrey, K. N., Leppla, C. A., Wichmann, R., Neve, R., Wildes, C. P. & Tye, K. M. (2015) Decoding neural circuits that control compulsive sucrose seeking. Cell, **160,** 528–541.

Oliva, I. & Wanat, M. J (2016) Ventral tegmental area afferents and drug-dependent behaviors. Front Psychiatry **7,** 30.

Papathanou, M., Creed, M., Dorst, M. C., Bimpisidis, Z. , Dumas, S., Pettersson, H., Bellone, C., Silberberg, G., Lüscher, C. & Wallén-Mackenzie, A. (2018) Targeting VGLUT2 in mature dopamine neurons decreases mesoaccumbal glutamatergic transmission and identifies a role for glutamate co-release in synaptic plasticity by increasing baseline AMPA/NMDA ratio. Front. Neural Circuits, **12,** 64.

R Core Team (2018). R: A language and environment for statistical computing. R Foundation for Statistical Computing, Vienna, Austria. URL https://www.R-project.org./

Samuels, I. S., Saitta, S. C. & Landreth, G. E. (2009) MAP'ing CNS development and cognition: an ERKsome process. Neuron, **61,** 160–167.

Sokoloff, L., Reivich, M., Kennedy, C., Des Rosiers, M. H., Patlak, C. S., Pettigrew, K. D., Sakurada, O. & Shinohara, M. (1977) The [14C]Deoxyglucose method for the measurement of

local cerebral glucose utilisation: theory, procedure and normal values in the conscious anethetized albino rat. J. Neurochem., **28,** 897-916.

Spielewoy, C., Biala, G., Roubert, C., Hamon, M., Betancur, C. & Giros, B. (2001) Hypolocomotor effects of acute and daily d-amphetamine in mice lacking the dopamine transporter. Psychopharmacology, **159,** 2–9.

Thomas, G. M. & Huganir, R. L. (2004) MAPK cascade signalling and synaptic plasticity. Nat. Rev. Neurosci., **5,** 173–183.

Ungless, M. A., Whistler, J. L., Malenka, R. C. & Bonci, A. (2001) Single cocaine exposure in vivo induces long-term potentiation in dopamine neurons. Nature, **411,** 583–587.

Vithayathil, J., Pucilowska, J. & Landreth, G. E. (2018) ERK/MAPK signaling and autism spectrum disorders. Prog. Brain Res., **241,** 63-112.

Walsh, J. J. & Han, M. H. (2014) The heterogeneity of ventral tegmental area neurons: Projection functions in a mood-related context. Neuroscience, **282C,** 101–108.

Yasuda, S., Sugiura, H., Tanaka, H., Takigami, S. & Yamagata, K. (2011) p38 MAP kinase inhibitors as potential therapeutic drugs for neural diseases. Cent. Nerv. Syst. Agents Med. Chem., **11,** 45–59.

Figure Captions

Figure 1. Altered VTA metabolism and functional connectivity in MKP-2$^{-/-}$ mice. (a) LCGU is selectively increased in the VTA of MKP-2$^{-/-}$ mice (n = 11) compared to MKP-2$^{+/+}$ control mice (n = 10) but not in (b) the ventral hippocampal CA1 region or (c) the central amygdala. (d-i) Summary statistical diagrams showing altered VTA functional connectivity in MKP-2$^{-/-}$ mice. Brain section figures are modified from the Allen mouse brain atlas (http://mouse.brain-map.org/static/atlas). Blue denotes regions that have significantly lost functional connectivity with the VTA in MKP-2$^{-/-}$ mice. Red denotes regions that show significantly gained functional connectivity to the VTA in MKP-2$^{-/-}$ but not MKP-2$^{+/+}$ mice. Yellow highlights the anatomical localisation of the VTA. (j) The functional connectivity heatmap also shows the lost (blue) and gained (red) alterations in VTA functional connectivity in MKP2-/- mice. Amyg. = Amygdala, Dorsal Hip.= Dorsal Hippocampus, Ventral Hip.= Ventral Hippocampus, Aud. = Auditory System, Multi.= Mutlimodal regions. Regional abbreviations and their systems are shown in Table 1. Differences in LCGU between groups was analysed using unpaired two-tailed Student's t-test with * $p < 0.05$ vs MKP-2$^{+/+}$ controls. Full LCGU and functional connectivity data are shown in Tables 1 and 2 respectively.

Figure 2. Increased sEPSC frequency onto VTA DA neurons in MKP-2$^{-/-}$ mice. (a) Representative images and traces of co-localisation of biocytin (magenta) filled I_H positive neuron and tyrosine hydroxylase (TH; green) in the VTA. (b-c) Representative I_H traces recorded from MKP-2$^{+/+}$ and MKP-2$^{-/-}$ VTA neurons respectively. (d) I_H amplitude is unaffected in VTA DA neurons from MKP-2$^{-/-}$ mice when compared to MKP-2$^{+/+}$ controls (n = 6). (e-f) Representative sEPSC traces from MKP$^{+/+}$ and MKP$^{-/-}$ mice respectively. (g) sEPSC frequency is increased in MKP-2$^{-/-}$ slices (n = 6) compared to MKP$^{+/+}$ slices (n = 6) whereas (h) sEPSC amplitude is unchanged. Data were analysed using 2-way repeated-measures ANOVA followed

by Bonferroni *post-hoc* correction (I_H) and two-tailed Mann-Whitney U non-parametric tests (sEPSCs) with * $p < 0.05$ *vs* MKP-$2^{+/+}$ controls. N is equal to one neuron per slice per animal with all I_H positive neurons confirmed to be DA neurons (TH positive) post experiment.

Figure 3. No change in dopamine neuron number in MKP-$2^{-/-}$ mice. (**a)** Immunostaining for tyrosine hydroxylase (TH; green) and DAPI (blue) appeared normal in MKP-$2^{-/-}$ mice (n = 6) compared to MKP-$2^{+/+}$ control mice (n=6). (b) Quantitative analyses revealed no significant differences between the densities of dopaminergic (TH+ve) neurons, total cell bodies (DAPI) and the ratio of TH / total cells in MKP-$2^{-/-}$ mice compared to MKP-$2^{+/+}$ control mice. Data analysed using unpaired two-tailed Student's t-tests.

Figure 4. Reduced amphetamine-induced hyperlocomotion but increased sucrose preference in MKP-$2^{-/-}$ mice. (a) Amphetamine (3mg kg^{-1}, i.p.)-induced hyperlocomotion is significantly attenuated in MKP-$2^{-/-}$ mice (n=8 for both genotypes). (b) Sucrose intake (1% solution) in relation to total fluid intake is significantly increased in MKP-$2^{-/-}$ mice compared to MKP-$2^{+/+}$ mice on trial days 2 and 3 (n=16 for both genotypes). Both sets of data were analysed using 2-way repeated-measures ANOVA followed by Bonferroni *post-hoc* correction with * $p < 0.05$ *vs* MKP-$2^{+/+}$ controls.

Table 1

Table 1. LCGU is increased in the VTA of MKP-2$^{-/-}$ mice.

	MKP-2$^{+/+}$			MKP-2$^{-/-}$			
	mean		S.E.	mean		S.E.	% difference
Prefrontal Cortex							
Lateral Orbital Cortex (LO)	1.64	±	0.04	1.64	±	0.03	0
anterior Prelimbic Cortex (aPrL)	1.15	±	0.03	1.18	±	0.02	2
Dorsolateral Orbital Cortex (DLO)	0.89	±	0.02	0.85	±	0.02	-5
Frontal Association Area (FRA)	1.20	±	0.02	1.16	±	0.02	-3
medial Prelimbic Cortex (mPrL)	1.14	±	0.03	1.14	±	0.03	0
Infralimbic Cortex (IL)	0.93	±	0.03	0.90	±	0.02	-3
Cingulate Cortex (Cg1)	1.22	±	0.03	1.26	±	0.02	4
Cortex							
Primary Motor Cortex (M1)	1.24	±	0.02	1.19	±	0.03	-4
Sensory Cortex Barrel Field (SC-BF)	1.31	±	0.03	1.34	±	0.05	2
Primary Somatosensory Cortex (S1)	1.33	±	0.03	1.23	±	0.04	-7
Piriform Cortex (Piri)	1.55	±	0.03	1.49	±	0.03	-4
Insular Cortex (Ins)	0.81	±	0.01	0.80	±	0.02	-2
Entorhinal Cortex (EntC)	0.92	±	0.02	0.91	±	0.02	-1
Primary Visual Cortex (V1)	1.20	±	0.05	1.28	±	0.05	7
Mesolimbic System							
Ventral Tegmental Area (VTA)	1.24	±	0.03	1.33	±	0.03	7*
Nucleus Accumbens Core (NacC)	0.93	±	0.02	0.89	±	0.02	-4
Nucleus Accumbens Shell (NacS)	1.04	±	0.03	1.02	±	0.01	-1
Basal Ganglia							
Dorsolateral Striatum (DLST)	1.30	±	0.02	1.30	±	0.02	0
Ventromedial Striatum (VMST)	1.29	±	0.02	1.26	±	0.03	-3
Globus Pallidus (GP)	0.92	±	0.03	0.93	±	0.02	2
Substantia Nigra pars Reticulata (SNR)	0.81	±	0.02	0.81	±	0.02	0
Substantia Nigra pars Compacta (SNC)	1.06	±	0.03	1.05	±	0.02	-1
Thalamus							
Anteromedial Thalamus (AMthal)	1.64	±	0.05	1.68	±	0.03	3
Anteroventral Thalamus (AVthal)	1.80	±	0.05	1.85	±	0.05	3
Mediodorsal Thalamus (MDthal)	1.42	±	0.02	1.46	±	0.04	3
Venterolateral Thalamus (VLthal)	1.50	±	0.04	1.49	±	0.03	0
Centrolateral Thalamus (CLthal)	1.15	±	0.04	1.22	±	0.04	6
Ventromedial Thalamus (VMthal)	1.36	±	0.04	1.36	±	0.04	0
dorsal Reticular Thalamus (dRT)	1.10	±	0.03	1.17	±	0.04	7
Nucleus Reuniens (Re)	1.16	±	0.04	1.19	±	0.05	3
Amygdala							
Basolateral Amygdala (BLA)	0.87	±	0.03	0.86	±	0.02	-1
Central Amygdala (CeA)	0.87	±	0.02	0.84	±	0.02	-3
Medial Amygdala (MeA)	0.73	±	0.02	0.75	±	0.02	2

Table 1

Hippocampus								
Dorsal								
Dorsal Hippocampus -Molecular Layer (DH-ML)	1.27	±	0.04	1.27	±	0.04	0	
Dorsal Hippocampus-CA1 (DH-CA1)	0.84	±	0.02	0.86	±	0.03	2	
Dorsal Hippocampus-CA2 (DH-CA2)	0.78	±	0.02	0.77	±	0.02	-1	
Dorsal Hippocampus-CA3 (DH-CA3)	0.81	±	0.02	0.79	±	0.02	-3	
Dorsal Hippocampus-DG (DH-DG)	0.78	±	0.03	0.78	±	0.03	0	
Ventral								
Ventral Hippocampus-Dorsal Subiculum (VH-DS)	1.17	±	0.04	1.19	±	0.02	2	
Ventral Hippocampus-CA1 (VH-CA1)	0.96	±	0.04	0.95	±	0.02	-1	
Ventral Hippocampus-CA2 (VH-CA2)	0.87	±	0.02	0.85	±	0.02	-3	
Ventral Hippocampus-CA3 (VH-CA3)	0.68	±	0.02	0.68	±	0.02	-1	
Ventral Hippocampus-DG (VH-DG)	0.70	±	0.03	0.68	±	0.02	-2	
Ventral Hippocampus-ML (VH-ML)	1.11	±	0.03	1.08	±	0.02	-2	
Septum/Diagonal Band of Broca								
Medial Septum (MS)	0.94	±	0.03	0.91	±	0.02	-2	
Vertical Limb of the Diagonal Band of Broca (VDB)	1.02	±	0.02	1.00	±	0.02	-1	
Horizontal Limb of the Diagonal Band of Broca (HDB)	1.07	±	0.02	1.06	±	0.02	-1	
Auditory System								
Medial Geniculate (MG)	1.21	±	0.04	1.26	±	0.04	4	
Inferior Colliculus (IC)	2.17	±	0.10	2.12	±	0.09	-3	
Neuromodulatory								
Dorsal Raphé (DR)	0.87	±	0.03	0.90	±	0.02	4	
Median Raphé (MR)	1.18	±	0.03	1.19	±	0.03	1	
Multimodal								
Mamillary Body (MB)	1.74	±	0.04	1.74	±	0.05	0	
Lateral Habenula (LHab)	1.34	±	0.03	1.41	±	0.04	5	

Data shown as the mean ± S.E.M. ^{14}C-2-deoxyglucose uptake ratio. Data analysed using Student's t-test with * $p < 0.05$ vs MKP-2$^{+/+}$ controls, $n \geq 10$ mice per genotype.

Table 2

Table 2. Altered VTA Connectivity in MKP-2$^{-/-}$ mice

	MKP-2$^{+/+}$			MKP-2$^{-/-}$			p-value	t-value (df = 21)
	Mean		SE	Mean		SE		
Prefrontal Cortex								
Lateral Orbital Cortex (LO)	**0.92**	**±**	**0.03**	0.56	±	0.09	ns	
anterior Prelimbic Cortex (aPrL)	0.66	±	0.10	**1.07***	**±**	**0.04**	**0.042**	**2.166**
Dorsolateral Orbital Cortex (DLO)	0.45	±	0.05	**0.74***	**±**	**0.05**	**0.026**	**2.395**
Frontal Association Area (FRA)	**0.85**	**±**	**0.02**	**1.11**	**±**	**0.10**	ns	
medial Prelimbic Cortex (mPrL)	**0.96**	**±**	**0.03**	**1.20**	**±**	**0.10**	ns	
Infralimbic Cortex (IL)	**1.35**	**±**	**0.03**	0.69**	±	0.07	**0.005**	**-3.118**
Cingulate Cortex (Cg1)	**0.97**	**±**	**0.03**	0.75	±	0.06	ns	
Cortex								
Primary Motor Cortex (M1)	0.72	±	0.06	**1.30***	**±**	**0.10**	**0.010**	**2.831**
Sensory Cortex Barrel Field (SC-BF)	0.36	±	0.06	0.73	±	0.04	ns	
Primary Somatosensory Cortex (S1)	**1.14**	**±**	**0.03**	**1.30**	**±**	**0.09**	ns	
Piriform Cortex (Piri)	0.71	±	0.08	0.52	±	0.10	ns	
Insular Cortex (Ins)	**1.41**	**±**	**0.05**	0.67**	±	0.04	**0.005**	**-3.118**
Entorhinal Cortex (EntC)	**1.10**	**±**	**0.03**	**1.56****	**±**	**0.07**	**0.005**	**3.118**
Primary Visual Corex (V1)	**0.91**	**±**	**0.03**	0.68**	±	0.04	**0.005**	**-3.118**
Mesolimbic System								
Nucleus Accumbens Core (NacC)	**0.86**	**±**	**0.06**	0.69	±	0.05	ns	
Nucleus Accumbens Shell (NacS)	**0.96**	**±**	**0.09**	0.40**	±	0.07	**0.005**	**-3.118**
Basal Ganglia								
Dorsolateral Striatum (DLST)	**0.87**	**±**	**0.05**	**1.10**	**±**	**0.06**	ns	
Ventromedial Striatum (VMST)	0.39	±	0.05	**1.53****	**±**	**0.10**	**0.005**	**3.118**
Globus Pallidus (GP)	0.51	±	0.05	**1.20****	**±**	**0.10**	**0.005**	**3.118**
Substantia Nigra pars Reticulata (SNR)	**1.22**	**±**	**0.04**	0.54**	±	0.11	**0.005**	**-3.118**
Substantia Nigra pars Compacta (SNC)	**1.38**	**±**	**0.02**	**2.59****	**±**	**0.07**	**0.005**	**3.118**
Thalamus								
Anteromedial Thalamus (AMthal)	0.61	±	0.07	0.55	±	0.07	ns	
Anteroventral Thalamus (AVthal)	0.60	±	0.10	**1.16****	**±**	**0.07**	**0.005**	**3.118**
Mediodorsal Thalamus (MDthal)	0.69	±	0.04	**0.83**	**±**	**0.05**	ns	
Venterolateral Thalamus (VLthal)	**1.25**	**±**	**0.05**	**1.01**	**±**	**0.06**	ns	
Centrolateral Thalamus (CLthal)	**1.44**	**±**	**0.02**	0.82**	±	0.06	**0.005**	**-3.118**
Ventromedial Thalamus (VMthal)	**1.47**	**±**	**0.01**	**1.01****	**±**	**0.07**	**0.005**	**3.118**
dorsal Reticular Thalamus (dRT)	0.40	±	0.08	0.49	±	0.05	ns	
Nucleus Reuniens (Re)	**0.91**	**±**	**0.02**	**1.04**	**±**	**0.07**	ns	
Amygdala								
Basolateral Amygdala (BLA)	**1.48**	**±**	**0.03**	0.79**	±	0.05	**0.005**	**-3.118**
Central Amygdala (CeA)	0.58	±	0.06	0.48	±	0.04	ns	
Medial Amygdala (MeA)	**1.23**	**±**	**0.04**	**0.95***	**±**	**0.06**	**0.005**	**3.118**

Table 2

Hippocampus										
Dorsal										
Dorsal Hippocampus -Molecular Layer (DH-ML)	**0.85**	±	**0.04**	**1.14***	±	**0.05**	**0.010**	**2.831**
Dorsal Hippocampus-CA1 (DH-CA1)	**1.14**	±	**0.02**	0.68**	±	0.06	**0.005**	**-3.118**
Dorsal Hippocampus-CA2 (DH-CA2)	**1.26**	±	**0.03**	**1.26**	±	**0.04**	ns	
Dorsal Hippocampus-CA3 (DH-CA3)	**1.20**	±	**0.05**	**0.96**	±	**0.06**	ns	
Dorsal Hippocampus-DG (DH-DG)	**0.82**	±	**0.03**	**1.40****	±	**0.04**	**0.005**	**3.118**
Ventral								
Ventral Hippocampus-Dorsal Subiculum (VH-DS)	**1.19**	±	**0.01**	0.45**	±	0.05	**0.005**	**-3.118**
Ventral Hippocampus-CA1 (VH-CA1)	**0.88**	±	**0.03**	0.70	±	0.07	ns	
Ventral Hippocampus-CA2 (VH-CA2)	**0.90**	±	**0.03**	**1.00**	±	**0.06**	ns	
Ventral Hippocampus-CA3 (VH-CA3)	**0.85**	±	**0.04**	0.81	±	0.08	ns	
Ventral Hippocampus-DG (VH-DG)	0.73	±	0.04	**0.90**	±	**0.06**	ns	
Ventral Hippocampus-ML (VH-ML)	**1.09**	±	**0.04**	**1.06**	±	**0.16**	ns	
Septum/Diagonal Band of Broca								
Medial Septum (MS)	**1.34**	±	**0.04**	**1.17**	±	**0.05**	ns	
Vertical Limb of the Diagonal Band of Broca (VDB)	0.31	±	0.06	0.45	±	0.08	ns	
Horizontal Limb of the Diagonal Band of Broca (HDB)	0.60	±	0.04	0.56	±	0.04	ns	
Auditory System								
Medial Geniculate (MG)	0.81	±	0.07	0.64	±	0.04	ns	
Inferior Colliculus (IC)	**0.97**	±	**0.03**	0.62**	±	0.05	**0.005**	**-3.118**
Neuromodulatory								
Dorsal Raphé (DR)	0.80	±	0.06	0.63	±	0.04	ns	
Median Raphé (MR)	**0.99**	±	**0.07**	0.64*	±	0.06	**0.042**	**-2.166**
Multimodal								
Mamillary Body (MB)	**1.66**	±	**0.08**	0.74**	±	0.05	**0.005**	**-3.118**
Lateral Habenula (LHab)	0.78	±	0.07	0.81	±	0.04	ns	

Data shown as the mean ± S.E.M of the VIP statistic gained from PLSR analysis. Bold denotes those RoI considered to be functionally connected to the VTA within each experimental group (where the 95% confidence interval of the VIP statistic for a given region exceeds the 0.8 threshold). Data analysed using Student's t-test with Bonferroni correction. * denotes $p < 0.05$ and ** denotes $p < 0.01$ significant difference in the VIP statistic in MKP-2$^{-/-}$ mice relative the MKP-2$^{+/+}$ controls. Only RoI showing significantly altered functional connectivity to the VTA in MKP-2$^{-/-}$ mice are shown. $n \geq 10$ mice per genotype.

Figure 1

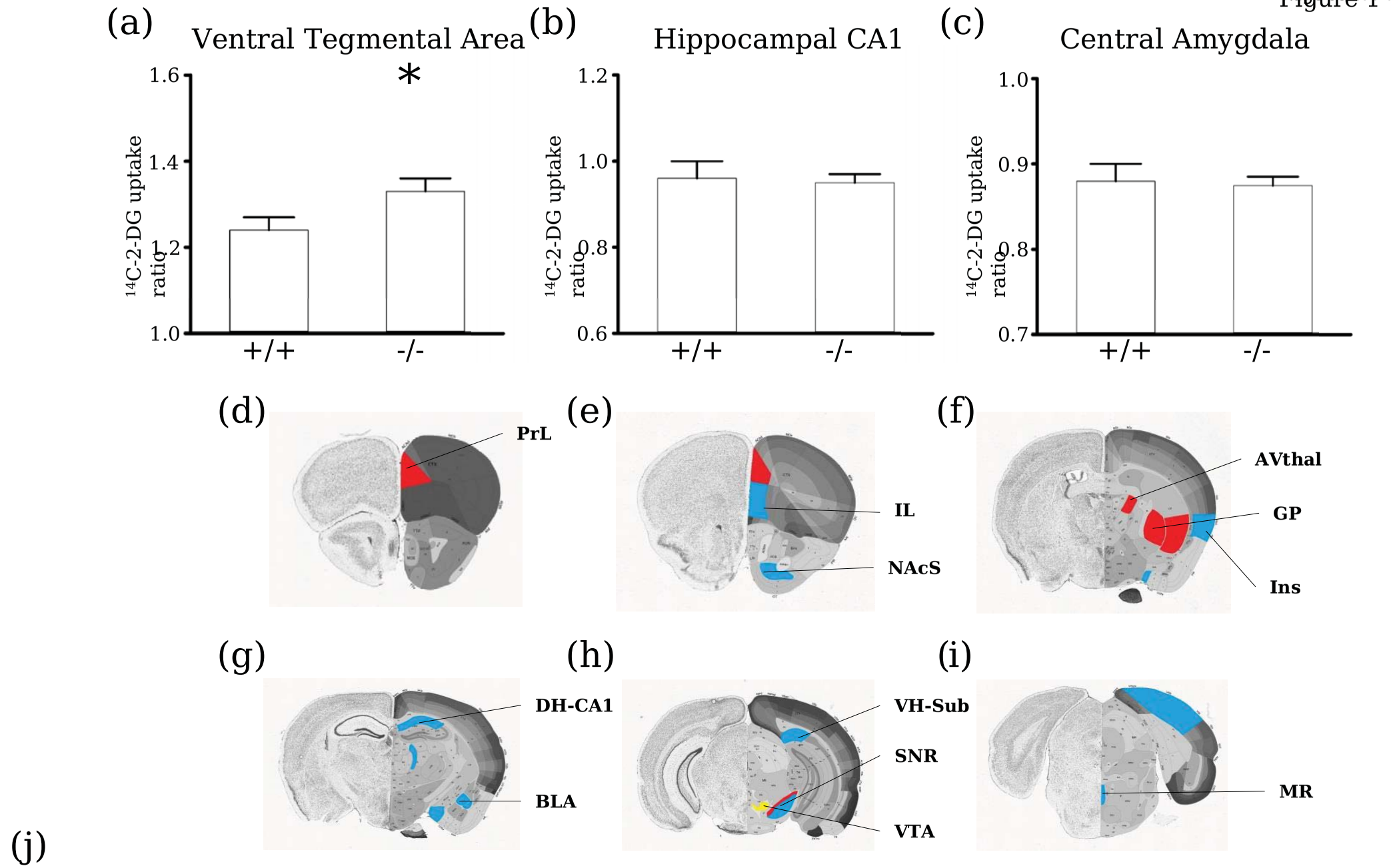
(a)
Ventral Tegmental Area
*
1.6
1.4
1.2
1.0
14C-2-DG uptake ratio
+/+
-/-
(b)
Hippocampal CA1
1.2
1.0
0.8
0.6
14C-2-DG uptake ratio
+/+
-/-
(c)
Central Amygdala
1.0
0.9
0.8
0.7
14C-2-DG uptake ratio
+/+
-/-
(d)
PrL
(e)
IL
NAcS
(f)
AVthal
GP
Ins
(g)
DH-CA1
BLA
(h)
VH-Sub
SNR
VTA
(i)
MR
(j)
Prefrontal Cortex
Cortex
Meso.
Basal Ganglia
Thalamus
Amyg.
Dorsal Hipp.
Ventral Hipp.
Septum
Aud.
5-HT
Multi.
LO aPrL DLO FRA mPrL IL Cg1
M1 SC-BF S1 Piri Ins EntoC V1
NacC NacS
DLST VMST GP SNR SNC
AMthal AVthal MDthal VLthal CLthal VMthal dRT Re
BLA CeA MeA
DH.ML DH.CA1 DH.CA2 DH.CA3 DH.DG
VH.DS VH.CA1 VH.CA2 VH.CA3 VH.DG VH.ML
MS VDB HDB
MG IC
DR MR
MB LatHab
VTA

Figure2

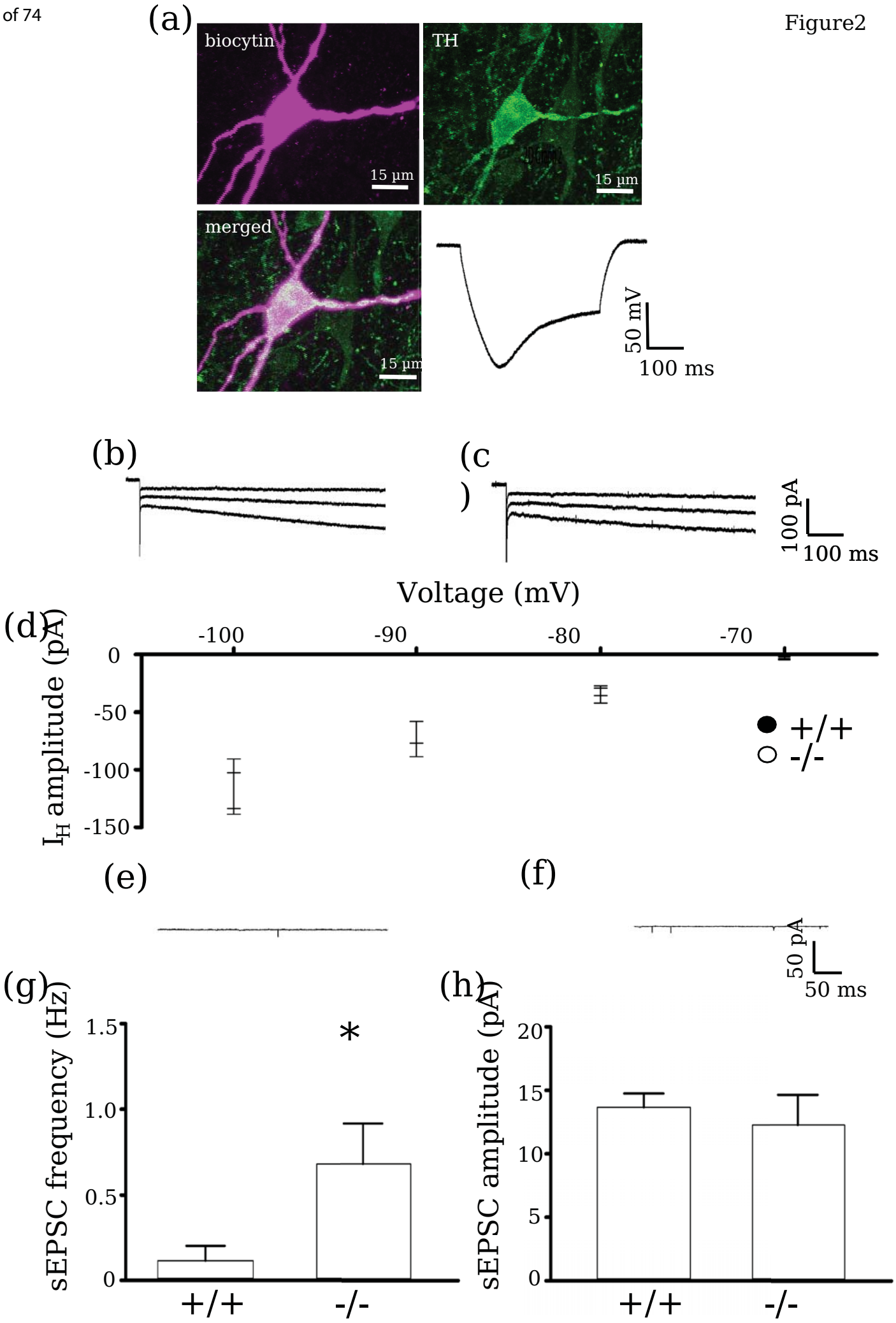
(a)
biocytin
15 µm
TH
15 µm
merged
15 µm
50 mV
100 ms
(b)
(c)
100 pA
100 ms
Voltage (mV)
(d)
-100
-90
-80
-70
0
-50
-100
-150
I_H amplitude (pA)
+/+
-/-
(e)
(f)
50 pA
50 ms
(g)
sEPSC frequency (Hz)
1.5
1.0
0.5
0
*
+/+
-/-
(h)
sEPSC amplitude (pA)
20
15
10
5
0
+/+
-/-

Figure3

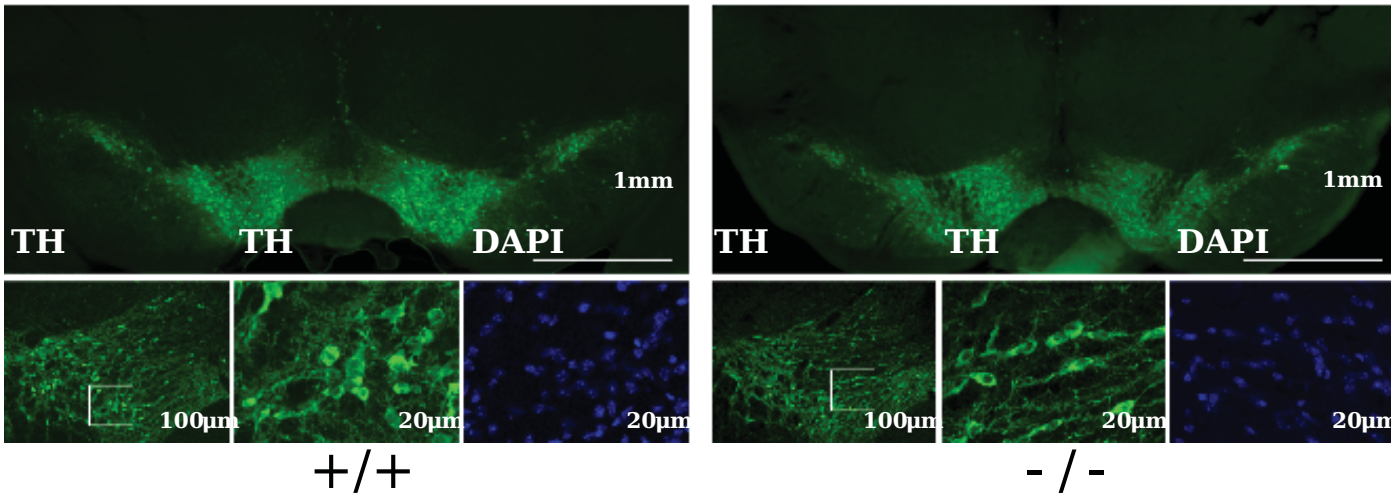
(a)
TH
TH
DAPI
1mm
100µm
20µm
20µm
+/+
- / -

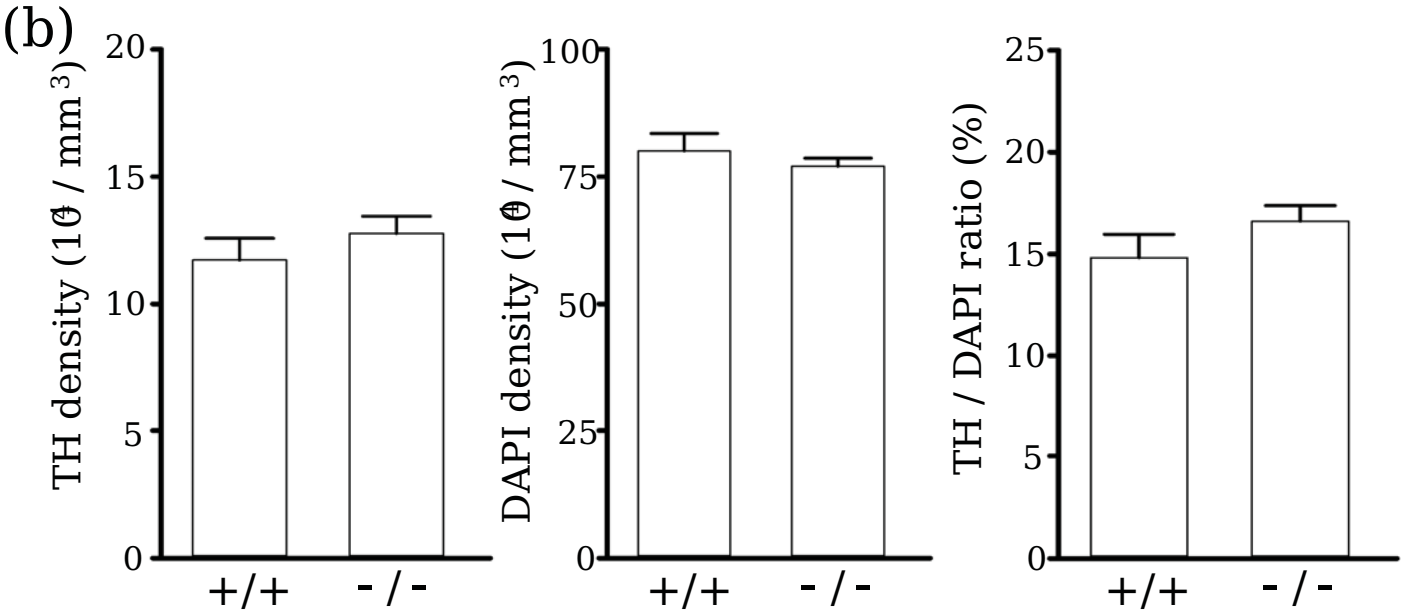
(b)
TH density (10⁴ / mm³)
DAPI density (10⁶ / mm³)
TH / DAPI ratio (%)
+/+
- / -

Figure 4

a

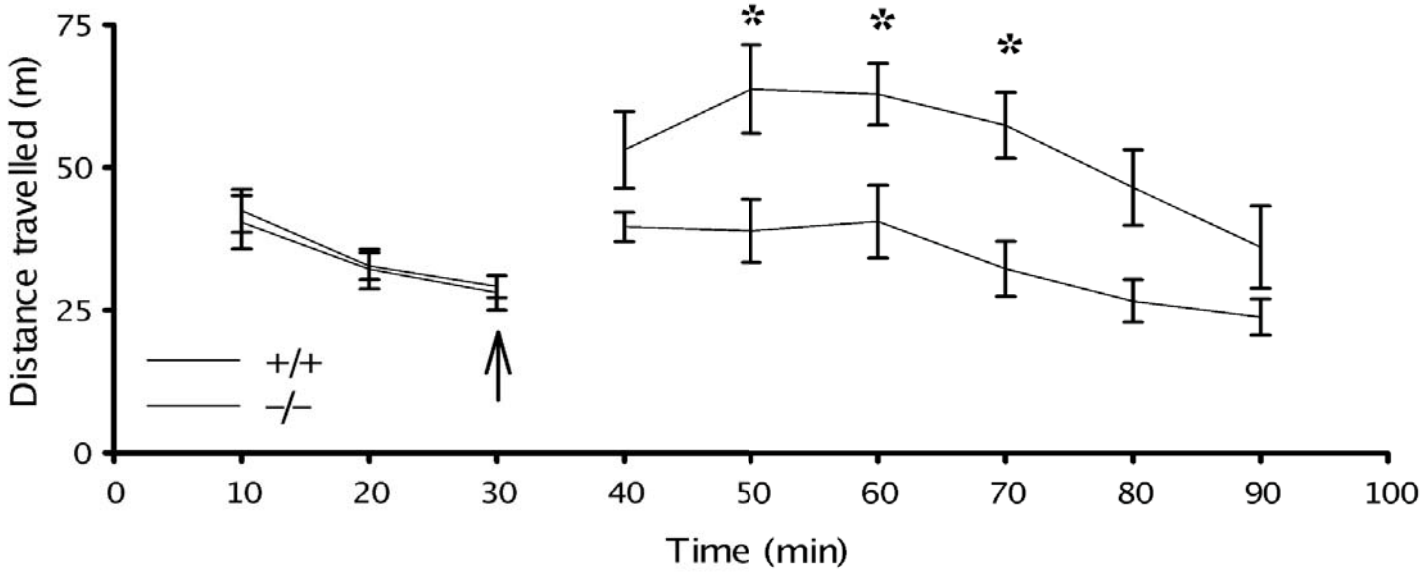
Distance travelled (m)
75
50
25
0
0
10
20
30
40
50
60
70
80
90
100
Time (min)
+/+
−/−
*
*
*

b

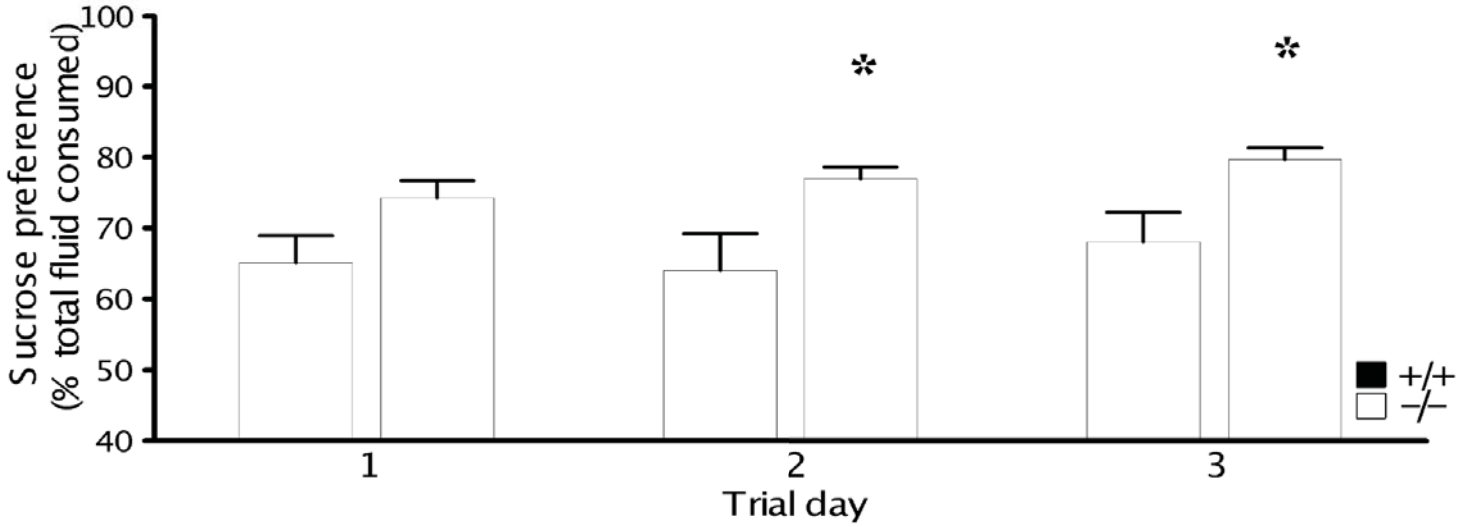
Sucrose preference
(% total fluid consumed)
100
90
80
70
60
50
40
1
2
3
Trial day
*
*
+/+
−/−

Supplementary Table 1 – Representative Shapiro-Wilk normality tests for data presented in figures 1-4.

Figure 1: Local cerebral glucose utilisation and functional brain connectivity analysis.				
Region	W-statistic	P value	Pass / fail	Statistical test used
VTA +/+	0.904	0.207	Pass	two-tailed unpaired t-test
VTA -/-	0.867	0.093	Pass	
Hippo +/+	0.630	0.630	Pass	two-tailed unpaired t-test
Hippo -/-	0.356	0.356	Pass	
CeA +/+	0.272	0.272	Pass	two-tailed unpaired t-test
CeA -/-	0.833	0.833	Pass	
Figure 2: Electrophysiological data				
sEPSC amplitude +/+	0.971	0.899	Pass	two-tailed unpaired t-test
sEPSC amplitude -/-	0.896	0.353	Pass	
sEPSC frequency +/+	0.587	<0.001	Fail	two-tailed Mann-Whitney U test
sEPSC frequency -/-	0.855	0.174	Pass	
Figure 3: Immunohistochemistry data				
TH density +/+	0.923	0.529	Pass	two-tailed unpaired t-test
TH dens -/-	0.929	0.574	Pass	
DAPI density +/+	0.235	0.235	Pass	two-tailed unpaired t-test
DAPI density -/-	0.902	0.902	Pass	
TH/DAPI +/+	0.578	0.578	Pass	two-tailed unpaired t-test
TH/DAPI -/-	0.146	0.146	Pass	
Figure 4: Sucrose preference test				
SPT day 1 +/+	0.926	0.210	Pass	two-tailed unpaired t-test
SPT day 1 -/-	0.914	0.135	Pass	
SPT day 2 +/+	0.952	0.529	Pass	two-tailed unpaired t-test
SPT day 2 -/-	0.951	0.501	Pass	
SPT day 3 +/+	0.953	0.541	Pass	two-tailed unpaired t-test
SPT day 2 -/-	0.951	0.511	Pass	

We examined whether the mitogen-activated protein kinase phosphatase (MKP-2) plays a global role in modulating brain function. Using MKP-2$^{-/-}$ mice, we reveal that ventral tegmental area (VTA) function and connectivity is altered, which is associated with increased excitatory drive onto VTA DA neurons but no change in VTA structure. In addition, behavioural tests indicate that MKP-2 plays a role in reward processing. Hence, we suggest that MKP-2 plays a role in modulating VTA function.

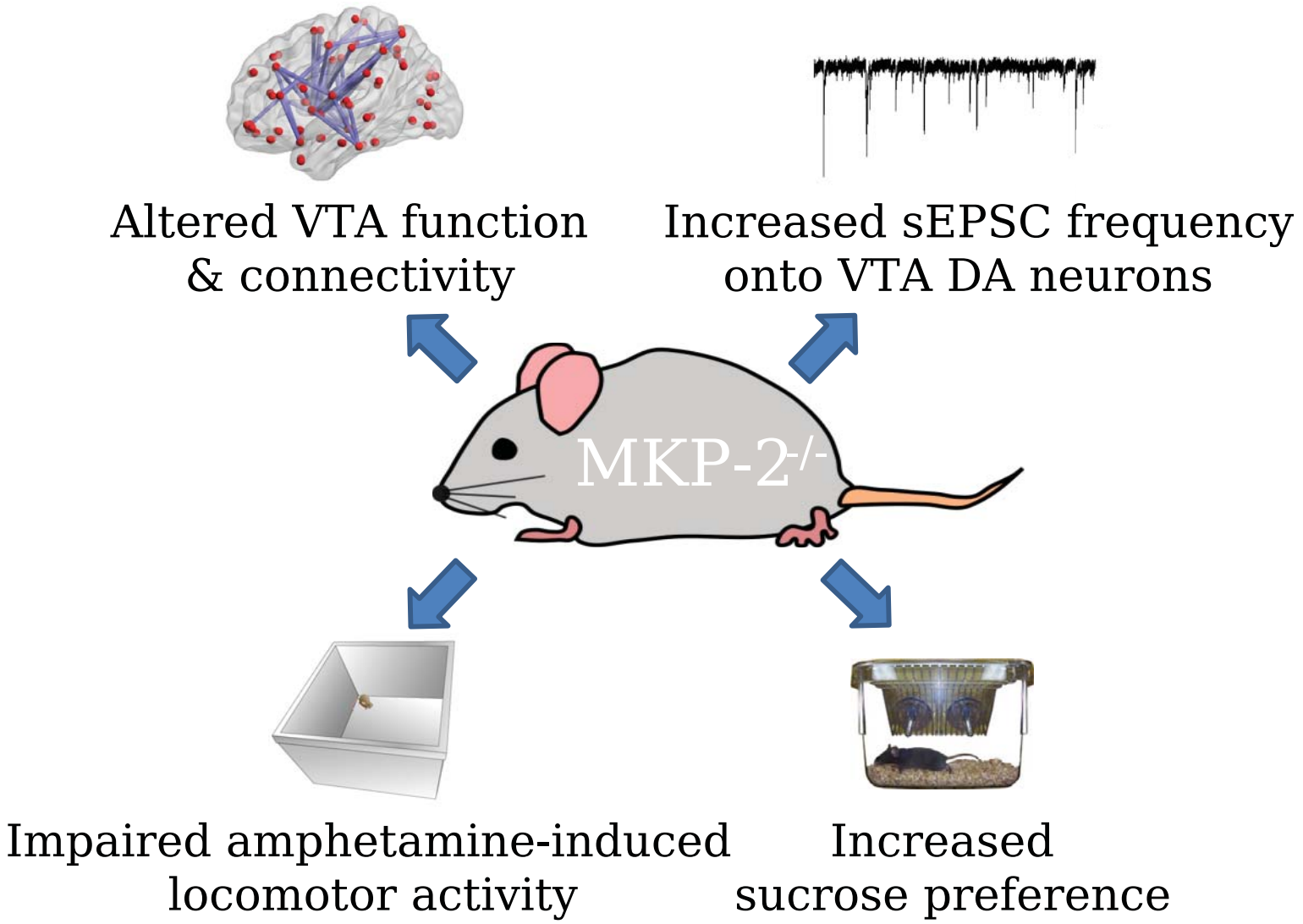
Altered VTA function
& connectivity
Increased sEPSC frequency
onto VTA DA neurons
MKP-2-/-
Impaired amphetamine-induced
locomotor activity
Increased
sucrose preference